Meson Spectra from a Dynamical Three-Field Model of AdS/QCD

A THESIS
SUBMITTED TO THE FACULTY OF THE GRADUATE SCHOOL
OF THE UNIVERSITY OF MINNESOTA
BY

Sean Peter Bartz

IN PARTIAL FULFILLMENT OF THE REQUIREMENTS
FOR THE DEGREE OF
DOCTOR OF PHILOSOPHY

Joseph I. Kapusta

August, 2014

Acknowledgements

There are many people that have earned my gratitude for their contribution to my time in graduate school. First, I would like to thank my adviser, Joe Kapusta, for taking a chance on a young graduate student, and for guiding my research during my time at Minnesota.

I would also like to thank Tom Kelley, who helped guide me through the beginnings of my research and helped me understand the basics of the AdS/CFT correspondence.

My graduate school experience was shaped by my participation in the Department of Energy Office of Science Graduate Fellowship for three years. The research support for travel made my graduate career a great experience, and the camaraderie with the other fellows was also fulfilling. I would like to thank Dr. Ping Ge, Cayla Stephenson, Igrid Gregory, and everyone else who made the DOE SCGF program a fulfilling, eye-opening experience.

This research is supported by the Department of Energy Office of Science Graduate Fellowship Pro- gram (DOE SCGF), made possible in part by the American Recovery and Reinvestment Act of 2009, administered by ORISE-ORAU under contract no. DE-AC05-06OR23100, by the US Department of Energy (DOE) under Grant No. DE-FG02-87ER40328, and by a Doctoral Dissertation Fellowship from the University of Minnesota.

Dedication

To my parents, Larry and Colleen, my first teachers. To my sister, Haley, my first student. To my wife, Alicia, my greatest support.

Abstract

Gauge/gravity dualities are a tool that allow the analytic analysis of strongly-coupled gauge theories. The Anti-de Sitter Space/Conformal Field Theory conjecture posits a duality between ten-dimensional string theory and a super Yang-Mills theory. A phenomenologically-motivated modification of this correspondence is known as AdS/QCD, a duality between strongly-coupled QCD-like theories and weakly-coupled gravitational theories in an additional dimension. QCD is not scale-invariant, so the dual theory must be modified in the conformal dimension to reflect this.

This thesis examines "soft-wall" models of AdS/QCD, wherein the conformal symmetry is broken by a field known as a dilaton. The dynamics of the dilaton and other background fields are examined, and a potential for these fields is determined. The background fields are numerically derived from this potential and used in the calculation of meson spectra, which match well to experiment.

The work presented here is based upon previously-published work by the author:

Contents

List of Tables

List of Figures

Chapter 1

Introduction

It's turtles
all the way down.
–Unknown

Each of the four fundamental forces of the universe is described by a particular theory. Gravity is understood through the techniques of general relativity, while electromagnetism and the weak nuclear force are united in the electroweak theory of the standard model. Quantum chromodynamics (QCD) describes the behavior of the strong nuclear force, which is the subject of this thesis.

The strong nuclear force binds together the constituents of nuclear matter. The fundamental constituents of the theory are quarks and the force-carrying particles known as gluons. The strength of an interaction is characterized by a parameter known as the coupling constant. Traditional perturbation techniques involve a series expansion in this constant, which works well when the coupling constant is small. When the coupling constant is large, each successive term in this expansion is larger than the preceding one, so the perturbation expansion is not useful. The value of the coupling constant of QCD varies with energy scale. At high energies, the coupling constant is small, but the strength of the interaction grows at lower energies. At these energies, quarks and gluons are confined within particles known as hadrons, and investigating their dynamics requires new techniques.

Beginning in the late 1990's, new techniques were proposed to tackle these non-perturbative problems. In the framework of string theory it was conjectured that a duality exists between strongly-coupled gauge theories and weakly-coupled gravitational theories. Calculations that are analytically intractable in the field theory can be related to more easily calculated results from the gravity theory. These models are known as gauge/gravity dualities. There has been recent excitement about results testing the duality by calculating the equivalent quantity on both sides of the duality, with positive results [2, 3]. While not a proof of the correspondence, this result impressively supports the validity of ongoing efforts into developing such theories.

One proposed gauge/gravity model is the AdS/CFT (Anti-de Sitter space/Conformal Field Theory) correspondence, which relates certain strongly-coupled field theories to weakly-coupled gravitational theories with an extra dimension. The potential application of the AdS/CFT correspondence to non-perturbative aspects of QCD was quickly recognized, although there are some assumptions in the correspondence that do not apply to QCD. While a gravitational dual to QCD has not been discovered, there has been much success over the past fifteen years in developing five-dimensional models that capture key features of hadron phenomenology. These effective models are known as AdS/QCD.

This thesis is organized as follows

- In Chapter 2, we introduce the AdS/CFT duality by reviewing the existing literature and presenting an argument for the correspondence.

- In Chapter 3, we describe previous work done on soft-wall AdS/QCD models. We cover the application of the model to the calculation of meson spectra and the modeling of chiral symmetry breaking. We discuss one particular modification to the simplest soft-wall model that accurately describes the explicit and spontaneous breaking of chiral symmetry. The application of this model to the pseudoscalar sector of mesons was contributed to by the author [4].

- In Chapter 4, we review the literature on dynamical models of AdS/QCD. This includes gravity-dilaton and gravity-dilaton-tachyon models.

- In Chapter 5, we detail the construction of a three-field dynamical AdS/QCD model. The need for a third background field is motivated by the analysis of chiral

symmetry breaking. We derive the equations of motion for the background fields, and construct a potential with the correct behavior. We describe the numerical techniques needed to derive the form of the background fields from this potential. This model was originally described in a paper by the author [5].

- In Chapter 6, we present the mass spectra for the vector, axial-vector, and pseudoscalar mesons that result from the three-field dynamical AdS/QCD model. We describe the method for calculating the meson spectra and compare the model to experimental results, showing good agreement. These results were also presented in [5].

- In Chapter 7, we discuss the mixing of the scalar meson field with the scalar glueball field. The mass eigenvalues will also be found in a forthcoming publication.

- Finally, in Chapter 8, we discuss the major conclusions of this analysis, along with open questions and the future prospects of this research program.

Chapter 2

Background

listen: there's a hell
of a good universe next door; let's go
–e.e. cummings

In this chapter, we cover the background of gauge/gravity dualities and the AdS/CFT correspondence. Our focus is on the phenomenological applications of these models, so many of the technical details of the correspondence will not be presented here. A variety of review articles cover the topic in more mathematical detail [6, 7, 8, 9, **?**]. Once we have motivated the AdS/CFT correspondence, we will review the applications of the duality to hadronic physics. We discuss the two major approaches to alter the conformal field theory to more closely resemble quantum chromodynamics. We also introduce a scheme to put these models on a more consistent theoretical basis.

2.1 What is AdS/CFT?

The general principle of dualities is to describe the same physical systems with two different but equivalent theories. The goal of this approach is to find that one of the theories is more analytically tractable than the other, and therefore more useful in describing physical phenomena. The original work on the AdS/CFT correspondence began with a duality between ten-dimensional string theory on $AdS_5 \times S^5$ and $\mathcal{N} = 4$ Super Yang-Mills Theory. The details of the string theory are not crucial to the

understanding of the derivation of the correspondence. The constituents of the theory are extended objects known as p-branes, where p refers to the spatial dimension of the object. One-dimensional p-branes are more commonly known as strings, which can be either closed or open. Closed strings are propagate freely through space, while open strings have their endpoints on p-dimensional Dirichlet-branes (D-branes). These strings are characterized by their length l_s and the coupling constant g_s that describes the strength of their interactions. These parameters are are related to the D-dimensional Newton's constant

$$G_D \sim g_s^2 l_s^{D-2}. \tag{2.1}$$

The string length can also be related to the Regge slope parameter

$$\alpha' = l_s^2. \tag{2.2}$$

We motivate the AdS/CFT correspondence by examining a stack of N D3 branes as a background for a type IIB string theory. We consider the dynamics of this system by taking the limits of low energy and strong coupling. The order in which these limits are taken determines the appearance of the result, yielding the two sides of the duality.

Taking the low-energy limit first gives an $SU(N)$ gauge theory, $\mathcal{N} = 4$ Super Yang-Mills (SYM) Theory. [1] The gauge coupling in this theory is related to the string coupling by

$$g_{YM}^2 = 4\pi g_s. \tag{2.3}$$

Assuming the string length is small, any interactions involving the open strings in the bulk (the region away from the branes) can be ignored. We are now free to make the assumption of strong coupling in the SYM theory. There are now two decoupled components of the low-energy system: the string theory governing the open strings in the bulk, and the strongly-coupled SYM theory on the branes.

Now, let us take the strong coupling limit first. In this instance, we have a large number of coincident D-branes resulting in a large energy density, and we must use general relativity to take into account its effect on the curvature of spacetime. The

[1] N.B. N refers to the number of D3 branes and the number of colors in the gauge theory, while $\mathcal{N}$ indicates the number of supercharges in the SYM theory.

classical metric that solves the supergravity equations is

$$ds^2 = \frac{1}{\sqrt{1+\frac{L^4}{r^4}}}\left(-dt^2 + d\vec{x}^2\right) + \sqrt{1+\frac{L^4}{r^4}}(dr^2 + r^2 d\Omega_5), \tag{2.4}$$

where the curvature radius L sets the scale and is given by[10, 11]

$$L^4 = 4\pi g_s N \alpha'^2. \tag{2.5}$$

The vector $\vec{x}$ runs over three spatial dimensions, and $d\Omega_5$ is the five-dimensional angular element.

The stack of N D3 branes is located at $r = 0$, and to an observer located at $r = \infty$, any excitations near the branes appears to be low energy due to gravitational red-shifting. As a consequence, taking the low-energy limit is equivalent to taking the limit $r \ll L$. The metric becomes

$$ds^2 = \frac{r^2}{L^2}(-dt^2 + d\vec{x}^2) + \frac{L^2}{r^2}dr^2 + L^2 d\Omega_5, \tag{2.6}$$

where r is strictly positive. This metric is a product of five dimensional anti-de Sitter space with a five-dimensional sphere ($AdS_5 \times S_5$). We can re-write this metric using the coordinate transformation

$$z = \frac{L^2}{r}. \tag{2.7}$$

This transformation gives a metric with a single warp factor,

$$ds^2 = \frac{L^2}{z^2}\left(-dt^2 + d\vec{x}^2 + dz^2\right), \tag{2.8}$$

where $z > 0$, with a UV cut-off at an infinitesimal z-value, $z = z_0$. The closed string excitations in the bulk are decoupled from the excitations near the branes.

In each of these descriptions, we began with a stack of N D3 branes and ended with a low-energy, strongly-coupled system. Taking the low-energy limit first results in an $\mathcal{N} = 4$ SYM gauge theory, while taking the strong coupling limit first yields a system of excitations on an $AdS_5 \times S_5$ metric. Maldacena's conjecture is that these two systems should describe the same physics. Each system has closed strings in the bulk that are decoupled from the rest of the system, so the conjecture results in a proposed duality between the $\mathcal{N} = 4$ SYM theory and type IIB string theory in anti-de Sitter space.

This duality is particularly useful if we can ignore all stringy effects and treat the type IIB string theory as a classical supergravity theory on the metric (2.6). This approximation is valid if the string length is much less than the radius of curvature,

$$l_s \ll L. \tag{2.9}$$

We can relate these quantities to the Yang-Mills coupling using (2.2), (2.3), and (2.5), yielding

$$\frac{L^4}{l_s^4} = g_{YM}^2 N. \tag{2.10}$$

The quantity $g_{YM}N$ is known as the 't Hooft coupling, λ. Thus, the requirement that the string length be small is equivalent to requiring the 't Hooft coupling to be large, $\lambda \gg 1$. In other words, the classical approximation is valid when the dual gauge theory is strongly coupled. The 't Hooft coupling acts as the effective gauge coupling, which is often expressed as a scalar field called the dilaton, Φ, where

$$\Phi = \log \lambda. \tag{2.11}$$

The behavior of the dilaton field will take a central role in this thesis.

In summary, Maldacena conjectured that a ten-dimensional string theory is dual to $\mathcal{N} = 4$ super Yang-Mills theory. We showed that the regime in which stringy effects can be neglected is equivalent to the strong-coupling limit of the gauge theory. The usefulness of this duality is evident, because the strong-coupling regime of a gauge theory is the limit in which it is difficult to perform calculations. Conveniently, this regime is dual to the string theory regime where calculations are easy because they can be done classically.

For our purposes, we reduce the 10-dimensional metric (2.6) to a five-dimensional space by ignoring the S_5 manifold and keeping only the AdS_5 metric (2.8). It turns out that discarding S_5 removes the supersymmetry from the SYM theory, resulting in a non-supersymmetric conformal field theory. In the end, we have a duality between a classical gravity theory in five dimensional anti-de Sitter space and a four-dimensional conformal field theory, our AdS/CFT correspondence. It is this relationship between a field theory in four dimensions and a gravitational theory in five dimensions that lends these models the evocative name *holography*.

2.2 Applying AdS/CFT to Quantum Chromodynamics

Phenomenologists would like to apply gauge/theory dualities to physical theories like quantum chromodynamics, rather than supersymmetric Yang-Mills theories that do not directly relate to real-world phenomena. These theories are closely-related enough to encourage a variety of attempts to bridge this gap. To do so, we must examine the differences between SYM theories and QCD.

We have shown how to remove the supersymmetry aspect of the gauge theory in the correspondence in the preceding section, which is necessary because QCD is not supersymmetric. However, we are still left with a conformal field theory, with no intrinsic energy scale. QCD has an energy scale called Λ_{QCD}, which is related to the phenomenon of confinement. Confinement is caused by the running of the QCD coupling with respect to energy scale. Conformal field theories have coupling constants which do not run, and therefore are not confining. Finally, the Yang-Mills theory has $N \gg 1$, while N_c, the number of colors in QCD is 3. Despite these differences, there are a variety of approaches to adapt the AdS/CFT correspondence to apply to QCD.

2.3 Top-Down Approach

One approach, known as the top-down approach, consists of modifying the string theory in some way in an attempt to produce a gauge theory that more accurately models QCD. Models that break conformal symmetry can study confinement [**?**]. The pure gauge theory with N D3 branes consists of only gluons, leading to the insertion of D7 "flavor branes" in the bulk to include quarks in the theory. [12] Strings that begin and end on the D7 branes represent quark/anti-quark pairs. These strings lack color indices and are therefore color singlets because they do not begin and end on the D3 branes. The excitations of this system corresponds to hadronic states. A prominent example that adds flavor and chiral symmetry breaking to the confining models is the Sakai-Sugimoto model [13, 14].

2.4 Bottom-Up Approach

Another approach, known as bottom-up or AdS/QCD models, begin from a phenomenological viewpoint, modifying the existing AdS background to capture some essential features of QCD. Because of this motivation, it is not known whether such models could eventually be derived from string theory. However, it is useful to investigate AdS/QCD as an effective phenomenological model, as well as a means to gain insights that may help in constructing an eventual string theory dual.

The modifications to the AdS background are constructions imposed by hand to introduce features such as confinement and chiral dynamics. Fields that are dual to the operators of the field theory are introduced by hand into the bulk of the AdS background. A Lagrangian is constructed from these fields, and the Euler-Lagrange equations that result are the equations of motion of the gauge field excitations. The normalizable solutions to these equations of motion are the hadronic states of the theory. The masses of the excited states of the mesons are calculated immediately from these eigenvalue problems, and other factors including decay constants and form factors can be calculated as well.

The backgrounds of these bottom-up models are imposed by hand, and not dynamically generated from any equations of motion. They are not derived from string theory, nor is it likely that they could be somehow embedded within any such theory. Despite the *ad hoc* nature of these models, the phenomenological results are often accurate to 10% or better. Importantly, they also give insight into how to capture the major features of QCD, such as confinement and chiral symmetry breaking. There are two major approaches to AdS/QCD, distinguished by the means used to break the conformal symmetry.

The Hard Wall

The simplest way to break the conformal symmetry of the gauge theory is to impose a hard cutoff in the conformal (z) dimension. The model was proposed by [15] and further explored by [16, 17] These so-called hard-wall AdS/QCD models insert both a UV brane located at $z \to 0$ and an IR brane at

$$z_1 = \frac{1}{\Lambda_{QCD}}. \tag{2.12}$$

The fields can propagate only between these two branes. The confinement scale is introduced by the IR brane.

These hard-wall models capture a variety of features of QCD, including correlation functions and form factors. The major failing of the hard-wall model is in describing the spectrum of radially excited mesons. It is well established experimentally that these excited states scale as $m_n^2 \sim n$ as n becomes sufficiently large, a phenomenon known as linear Regge trajectories or linear confinement. Hard-wall models produce a spectrum with a $m_n \sim n$ scaling, in conflict with experiment.

The Soft Wall

Instead of cutting off the metric, soft-wall models insert a z-dependent scalar dilaton field that breaks the conformal symmetry by acting as an effective cutoff. This model was proposed in [18] and further explored in [19, 20, 21, 22, 23, 24]. The dilaton multiplies the Lagrangian

$$\mathcal{S} = \int d^5x \mathrm{e}^{-2\Phi}\sqrt{-g}\mathcal{L}, \tag{2.13}$$

modifying the equations of motion of the fields contained in $\mathcal{L}$. A common and simple choice for the dilaton's behavior is a power-law,

$$\Phi = (\mu z)^\nu, \tag{2.14}$$

where μ introduces an energy scale into the model on the order of Λ_{QCD}. It was shown by Karch, *et al* [18] that a quadratic dilaton field

$$\Phi \sim z^2 \tag{2.15}$$

yields meson spectra with the desired $m_n^2 \sim n$ behavior. Because these linear Regge trajectories apply only when n becomes large, the power-law behavior is necessary strictly when z becomes large. Improved predictions for the lower meson states can be obtained by modifying the UV behavior of the dilaton field. Such modifications to this model were explored in [25]. The details of past work on soft-wall models will be explored further in Chapter 3.

2.5 Dynamical AdS/QCD

The early AdS/QCD models rely on parameterizations for the background fields such as the dilaton. A power law is the simplest choice for the dilaton's behavior, and was suggested in [18]. Later models including [25] improved phenomenology by modifying the dilaton in the UV limit. However, the models rely on *ad hoc* choices for the parameterization of the background fields and do not examine the dynamics of these fields.

So-called dynamical AdS/QCD models attempt a more rigorous examination of the vacuum dynamics of the dual model, as an attempt to remedy some of the shortcomings of the bottom-up approach discussed above [26, 27, 28, 29, 30, 31, 32]. These models examine terms in the Lagrangian involving the dilaton field as well as a tachyonic field that may be related to the chiral symmetry breaking of the model. Previous work examines the construction of the potential terms in the Lagrangian that will give rise to the desired behavior of the background fields. There has also been some work on examining meson spectra in dynamical AdS/QCD models, with some success.

2.6 Summary

In this chapter, we have presented the basics of AdS/CFT, including a conceptual motivation for the correspondence. We have also discussed the application of the correspondence to QCD, including the main research programs attempting to make this connection: the top-down and bottom-up approaches. Finally, we have introduced two areas of research in bottom-up AdS/QCD: the soft-wall model and dynamical AdS/QCD. These topics will be elaborated upon in the following chapters.

Chapter 3

Soft-Wall Model of AdS/QCD

Ad astra per alas porci.
To the stars on the wings of a pig.
–Motto on John Steinbeck's personal stamp

In this chapter, we will provide detail on previous work done on the soft-wall AdS/QCD model. We will present the set-up of the background metric and the fields that must be included in simplest version of the soft-wall model. The method for modeling the chiral symmetry breaking of QCD is discussed. The Euler-Lagrange equations for the gauge fields are derived, and the eigenvalue equations for the masses of the meson excited states are presented.

We will also describe work done to modify this soft-wall model to capture the correct form of chiral symmetry breaking by adding additional terms to the action. The changes to the meson equations of motion due to these additional terms are presented.

Finally, we present work on the pseudoscalar sector of the modified soft-wall model, contributed to by the author. Two alternative representations for the pseudoscalar field are presented and shown to be equivalent. We then calculate the meson spectrum for the pions and show that this model satisfies the Gell-Mann–Oakes–Renner relation.

3.1 Minimal Soft-Wall Model

The soft-wall model of AdS/QCD was introduced by Karch, *et al* [18] and studied further by [33, 19, 20, 21, 22, 23, 24]. This work showed that the behavior of highly-excited mesons is controlled by the infrared behavior of the AdS/CFT dual theory. They argued to replace the simple cut-off of the hard-wall model with a field known as the *dilaton* whose IR behavior would act as a smooth cut-off to the AdS space. In this section, we will describe the set-up and field content of such a simple model and compare the resulting behavior to that of a hard-wall model.

3.1.1 Metric and Field Content

The gravitational dual theory exists in five-dimensional anti-de Sitter space, with a metric given by

$$ds^2 g_{MN} dx^M dx^N = a^2(z)(\eta_{\mu\nu} dx^\mu dx^\nu + dz^2), \tag{3.1}$$

where $a(z) = L/z$ is the warp factor and L is the curvature radius of the anti-de Sitter space. We will often work in units where the curvature radius is unity. The Minkowski metric is given by

$$\eta_{\mu\nu} = \begin{pmatrix} -1 & 0 & 0 & 0 \\ 0 & 1 & 0 & 0 \\ 0 & 0 & 1 & 0 \\ 0 & 0 & 0 & 1 \end{pmatrix}. \tag{3.2}$$

The coordinate z has a range $0 \leq z < \infty$.

The bulk coordinate z is associated with inverse energy scales, with the ultraviolet limit of QCD represented by fields at $z \to 0$ [21]. The AdS/CFT dictionary [34, 35] states that each operator $\mathcal{O}(x)$ in the 4D conformal field theory is associated with a bulk field $\psi(x, z)$. The values of the bulk fields at the UV boundary act as sources for the corresponding 4D currents. Global symmetries of the 4D field theory become gauged symmetries for the bulk fields.

The generating functional of gauge-invariant operators of the gauge theory is dual to the minimum of the supergravity action. On the boundary, the supergravity fields must coincide with the sources of the gauge theory [36, 9]. That is,

$$\langle \mathrm{e}^{\int_{\partial AdS} d^4x\, \phi^0(\vec{x}) \mathcal{O}(\vec{x})} \rangle_{\mathrm{CFT}} = \mathrm{e}^{iS_{\mathrm{SUGRA}}(\phi)}|_{\phi=\phi_0}\ , \tag{3.3}$$

where ϕ^0 is a source term on the boundary of the five-dimensional supergravity (SUGRA) model. The gauge theory exists on the boundary, ∂AdS, of the dual gravitational theory. For each operator of conformal dimension Δ in the gauge theory, there is a coupling, $\phi^0\mathcal{O}$. For each of these terms, a scalar field with mass m is inserted into the AdS_5 gravity dual.

We can write down the Lagrangian of such a free massive scalar field,

$$\mathcal{L} = g^{MN}\partial_M\phi\partial_N\phi - m^2\phi^2. \tag{3.4}$$

The Euler-Lagrange equation is found by varying the action with respect to ϕ,

$$\begin{aligned}
\delta\mathcal{S} &= \delta\left(\sqrt{-g}g^{MN}\partial_M\phi\partial_N\phi - \sqrt{-g}m^2\phi^2\right) \\
&= \sqrt{-g}g^{\mu\nu}\partial_\mu\delta\partial_\nu\phi + \sqrt{-g}g^{zz}\partial_z\phi\delta\partial_z\phi - \sqrt{-g}m^2\phi\delta\phi \\
&= -a(z)^3\eta^{\mu\nu}\partial_\mu\partial_\nu\phi\delta\phi - \eta^{zz}\partial_z(a(z)^3\partial_z\phi\delta\phi) - a(z)^5m^2\phi\delta\phi \\
&= \left(z^5\partial_z(z^{-3}\partial_z\phi) + z^2\partial_i^2\phi - m^2\phi\right)\delta\phi,
\end{aligned} \tag{3.5}$$

resulting in the equation of motion

$$z^5\partial_z\left(z^3\partial_z\phi\right) + \left(m^2 + z^2\partial_i^2\right)\phi = 0. \tag{3.6}$$

Using the substitution $\partial_i^2\phi = -k^2\phi$, we can write this equation in momentum space

$$z^5\partial_z\left(z^{-3}\partial_z\phi\right) + \left(m^2 - k^2z^2\right)\phi = 0. \tag{3.7}$$

Near the $z = 0$ boundary, the k^2 term is neglected, and the asymptotic field behavior becomes [34, 37]

$$\phi \approx \phi^0 z^{\Delta_-} + \langle\mathcal{O}\rangle z^{\Delta_+}, \tag{3.8}$$

where the two solutions are

$$\Delta_\pm = \frac{d}{2} \pm \sqrt{\frac{d^2}{4} + m^2R^2}. \tag{3.9}$$

The mass is determined by the spatial dimension d and the operator dimension Δ

$$m^2 = \Delta(\Delta - d), \tag{3.10}$$

giving the two possible solutions of (3.9),

$$\Delta_+ = d, \tag{3.11}$$

$$\Delta_- = d - \Delta. \tag{3.12}$$

An operator $\mathcal{O}$ on the boundary may also be coupled to a p-form $\mathcal{C}$ in AdS space, via the coupling

$$\int_{M_d} \mathcal{C} \wedge \mathcal{O}. \tag{3.13}$$

In this case, the mass of the scalar field in the gravity dual is [37]

$$m^2 = (\Delta - p)(\Delta - p - d). \tag{3.14}$$

It seems that we should require $\Delta > p + d$, to avoid instabilities from tachyons with $m^2 < 0$. However, it has been shown [38] that tachyons with mass above the bound

$$m^2 > -\frac{d^2}{4} \tag{3.15}$$

are allowed.

The symmetries of the gauge field are also included in the gravitational dual through a prescription provided by the correspondence dictionary. A global symmetry of the gauge theory is represented represented by invariance under a transformation

$$U = \mathrm{e}^{i\eta}, \tag{3.16}$$

with η constant. This means that η should remain constant on the boundary of the gravity dual, but in the bulk, nothing prevents η from becoming a function of spacetime coordinates, x and z. The symmetry in the gravity dual is then represented by the transformation

$$U = \mathrm{e}^{i\eta(x,z)}. \tag{3.17}$$

In this way, the global symmetry of the gauge theory is represented by a local symmetry of the gravitational theory. A gauge field is inserted into the gravity dual for each relevant global symmetry.

For our AdS/QCD model, the field content of the five-dimensonal gravitational dual theory is dictated by the operators relevant to the chiral dynamics of QCD. The gauge fields L_μ, R_μ correspond to the left- and right-handed currents of the $SU(N_f)_L \times SU(N_f)_R$ chiral symmetry, where N_f is the number of quark flavors in the model. The scalar field X is associated with the chiral operator $\bar{q}q$ [15]. The masses of the bulk fields are set by the AdS/CFT relation [23]

$$m_5^2 L^2 = (\Delta - p)(\Delta + p - 4), \tag{3.18}$$

where Δ is the dimension of the p-form QCD operator. Table 3.1 illustrates the fields and operators of our model, showing that the scalar field is the only field in this model that is not massless.

4D Operator	5D Field	p	Δ	$m_5^2 L^2$
$\bar{q_L}\gamma^\mu t^a q_L$	L_μ^a	1	3	0
$\bar{q_R}\gamma^\mu t^a q_R$	R_μ^a	1	3	0
$\bar{q}_R^a q_L^b$	$\frac{2}{z}X^{ab}$	0	3	-3

Table 3.1: Operators and fields of the model. The matrices t^a are the generators of the $SU(N_f)$ symmetry.

The simplest soft-wall action involving the fields from Table 3.1 is given in [18] as

$$S_5 = \int d^5x\sqrt{-g}e^{-\Phi(z)}Tr\left[|DX|^2 + m_X^2|X|^2 + \frac{1}{4g_5^2}(F_L^2 + F_R^2)\right]. \tag{3.19}$$

The 5D gauge coupling constant g_5 is fixed by calculating the vector current two-point function using this model and then comparing this to the leading order result from QCD, leading to the identification $g_5^2 = 12\pi^2/N_c$. This calculation will be performed in Section 3.1.2.

The field X includes both the scalar and pseudoscalar fields, as well as a non-trivial vacuum expectation value (VEV)

$$X_e^{ab} = \left(\frac{\chi(z)}{2} + S^a(x,z)t^b\right) Ie^{2i\pi_e(x,z)^a t^b} \tag{3.20}$$

$$X_l^{ab} = \left(\frac{\chi(z)}{2} + S^a(x,z)t^b\right) I + i\pi_l(x,z)^a t^b, \tag{3.21}$$

with I the $N_f \times N_f$ identity matrix and t^a the $SU(N_f)$ generators, which are normalized as

$$\mathrm{Tr}[t^a t^b] = \delta^{ab}/2. \tag{3.22}$$

The indices a, b of the field X will be suppressed unless needed. The details of the representation choice will be discussed in Section 3.2.3. The field strength tensors are defined as

$$F_L^{MN} = \partial^M L^N - \partial^N L^M - i[L^M, L^N] \tag{3.23}$$

$$F_R^{MN} = \partial^M R^N - \partial^N R^M - i[R^M, R^N], \tag{3.24}$$

where we have used the shorthand notation $L^M = L^{Ma}t^a$. The covariant derivative becomes

$$D^M X = \partial^M X - iL^M X + iXR^M. \tag{3.25}$$

The physical vector (V) and axial-vector (A) fields are defined in terms of the L and R gauge fields

$$L^M = V^M + A^M, \tag{3.26}$$

$$R^M = V^M - A^M. \tag{3.27}$$

Substituting equations (3.26) and (3.27) into the last field strength tensors,

$$\begin{aligned} F_L^2 + F_R^2 &= 2\left(\partial^M L^N \partial_M L_N - \partial^M L^N \partial_N L_M + \frac{1}{2}[L^M, L^N][L_M, L_N]\right) \\ &+ 2\left(\partial^M R^N \partial_M R_N - \partial^M R^N \partial_N R_M + \frac{1}{2}[R^M, R^N][R_M, R_N]\right), \\ &= 4\left(\partial^M V^N \partial_M V_N - \partial^M V^N \partial_N V_M + \frac{1}{2}[V^M, V^N][V_M, V_N]\right) \\ &+ 4\left(\partial^M A^N \partial_M V_N - \partial^M A^N \partial_N A_M + \frac{1}{2}[A^M, A^N][A_M, A_N]\right), \\ &= 2\left(F_V^2 + F_A^2\right), \end{aligned} \tag{3.28}$$

where the vector and axial field-strength tensors have the form

$$F_V^{MN} = \partial^M V^N - \partial^N V^M - \frac{i}{\sqrt{2}}[V^M, V^N], \tag{3.29}$$

$$F_A^{MN} = \partial^M A^N - \partial^N A^M - \frac{i}{\sqrt{2}}[A^M, A^N]. \tag{3.30}$$

The covariant derivative can also be written in terms of the vector and axial fields

$$D_M X = \partial_M X - i\{A_M^a, X\} + i[V_M^a, X]. \tag{3.31}$$

This relation allows us to re-write the action (3.19),

$$S_5 = \int d^5x\sqrt{-g}e^{-\Phi(z)}Tr\left[|DX|^2 + m_X^2|X|^2 + \frac{1}{2g_5^2}(F_A^2 + F_V^2)\right]. \tag{3.32}$$

The scalar field X takes on a z-dependent vacuum expectation value (VEV), breaking the chiral symmetry. In a flavor-symmetric model, the VEV has the form

$$\langle X\rangle = \frac{\chi(z)}{2}I, \tag{3.33}$$

where I is the $N_f \times N_f$ identity matrix.

3.1.2 Equations of Motion

By varying the action (3.19), one obtains the equations of motion for the scalar, pseudoscalar, vector, and axial-vector mesons, as well as for the scalar vacuum expectation value.

Substituting the chiral field into the Lagrangian using (3.20), we vary the Lagrangian with respect to $\chi(z)$,

$$\begin{aligned}
\delta\mathcal{L}_{VEV} &= -\delta\left(\mathrm{e}^{-\Phi}\sqrt{-g}\,\mathrm{Tr}\left[\frac{g^{zz}}{4}\partial_z\chi\partial_z\chi + m_X^2\frac{\chi^2}{4}\right]\right) \\
&= -\delta\left(\frac{1}{2}\mathrm{e}^{-\Phi}a(z)^5\left(a(z)^{-2}\partial_z\chi\partial_z\chi + m_X^2\chi^2\right)\right) \\
&= -\mathrm{e}^{-\Phi}a(z)^3\partial_z\chi\delta\partial_z\chi - \mathrm{e}^{-\Phi}a(z)^5 m_X^2\chi\delta\chi \\
&= \left(\partial_z\left(\mathrm{e}^{-\Phi}a^3\partial_z\chi\right) - \mathrm{e}^{-\Phi}a^5 m_X^2\chi\right)\delta\chi, \qquad (3.34)
\end{aligned}$$

The equation of motion becomes

$$\partial_z^2\chi - \partial_z\Phi\partial_z\chi + \frac{\partial_z a(z)}{a(z)}\partial_z\chi - a(z)^2 m_X^2\chi = 0. \qquad (3.35)$$

In this model, the warp factor $a(z) = 1/z$ and the mass of the scalar field $m_X^2L^2 = -3$. With these substitutions, the equation of motion becomes

$$\chi'' - \Phi'\chi' - \frac{3}{z}\chi' + \frac{3}{z^2}\chi = 0. \qquad (3.36)$$

In the hard wall model, there is no dilaton, so we can set $\Phi' = 0$, finding the exact solution to (3.36) to be

$$\chi_{\mathrm{hw}}(z) = c_1 z + c_2 z^3, \qquad (3.37)$$

where c_1 and c_2 are integration constants. Comparing this solution to the UV behavior of the bulk fields in the AdS/CFT dictionary (3.8), c_1 and c_2 correspond to the source term and the operator expectation value, respectively,

$$c_1 \sim m_q, \qquad (3.38)$$

$$c_2 \sim \langle q\bar{q}\rangle \equiv \sigma. \qquad (3.39)$$

Here m_q is the quark mass and $\sigma = \langle\bar{q}q\rangle$ is the chiral condensate, the variation of the vacuum energy with respect to m_q.

In the simplest soft-wall model, it has been shown [18, 23] that the solution to (3.36) is given by

$$\chi_{sw}(z) = \frac{m_q}{L} z\,\Gamma\left(\frac{3}{2}\right) U\left(\frac{1}{2}, 0, \lambda z^2\right), \tag{3.40}$$

where $U(a, b, y)$ is the Tricomi confluent hypergeometric function. (There is also another solution that disregarded because it leads to an action that is not finite in the IR.) In the small-z limit, (3.40) expands to [23]

$$\chi_{sw}(z) \to \frac{m_q}{L} z - \frac{\lambda m_q}{2L} z^3 \left(1 - 2\gamma_E - 2\log(\sqrt{\lambda} z) - \psi\left(\frac{3}{2}\right)\right), \tag{3.41}$$

where ψ is the Euler function. However, comparing this solution to the UV behavior of the chiral condensate in the AdS/CFT dictionary (3.8), we see that $\sigma \sim m_q$. This is undesirable in a theory with spontaneous chiral symmetry breaking. In addition, when z becomes large, we see that the chiral condensate becomes a constant, $\chi \sim m_q$, linking the IR and UV behavior. As we will see, the IR behavior of the chiral field governs the behavior of the axial meson spectrum, another limitation of the solution (3.40). More generally, we can see that this issue is caused because the equation (3.36) is linear in χ. With only one normalizable solution, only one constant survives the application of boundary conditions. As a result, m_q and σ cannot be independent. To remedy this, it was suggested [18] to examine higher-order terms in the scalar potential. A particular example of this will be examined in Section 3.2, and a more general approach will be discussed in Chapter 4.

Scalar Sector

We now examine the fluctuations of the scalar field X, rather than its VEV, to determine the spectrum of the f_0 scalar mesons. We use the expression in (3.20), though it does not matter which representation for the pseudoscalar component of the field is used,

$$X(x, z) = \left(S(x, z) + \frac{\chi(z)}{2}\right) \mathrm{e}^{2i\pi(x,z)}. \tag{3.42}$$

To obtain the equations of motion, we vary the action with respect to the scalar field $S(x, z)$,

$$\delta\mathcal{L}_S \;=\; \delta\left(\mathrm{e}^{-\Phi}\sqrt{-g}\,\mathrm{Tr}\left[g^{MN}\partial_M S(x,z)\partial_N S(x,z) + m_X^2 S(x,z)^2\right]\right)$$

$$
\begin{aligned}
&= \delta\left(\mathrm{e}^{-\Phi}\sqrt{-g}\,\mathrm{Tr}(t^a t^b)\left(g^{\mu\nu}\partial_\mu S\partial_\nu S + g^{zz}\partial_z S\partial_z S + m_X^2 S^2\right)\right) \\
&= \mathrm{e}^{-\Phi}a(z)^3\eta^{\mu\nu}\partial_\mu S\,\delta\partial_\nu S + \mathrm{e}^{-\Phi}a(z)^3\partial_z S\,\delta\partial_z S + \mathrm{e}^{-\Phi}a(z)^5 m_X^2 S\,\delta S \\
&= \left(-\mathrm{e}^{-\Phi}a(z)^3\partial_\mu\partial^\mu S - \partial_z\left(\mathrm{e}^{-\Phi}a(z)^3\partial_z S\right) + \mathrm{e}^{-\Phi}a(z)^5 m_X^2 S\right)\delta S, \qquad (3.43)
\end{aligned}
$$

leaving the equation of motion,

$$\mathrm{e}^{\Phi}a^{-3}\partial_z\left(\mathrm{e}^{-\Phi}a^3\partial_z S\right) + \partial_\mu\partial^\mu S - a^2 m_X^2 S = 0. \qquad (3.44)$$

We separate the z-dependent part of the field by using Kaluza-Klein decomposition,

$$S(x,z) = \sum_{n=0}^{\infty} S_n(z)\mathcal{S}_n(x). \qquad (3.45)$$

We use the AdS warp factor $a(z) = 1/z$ and use Proca's equation

$$\partial_i\partial^i S_n = m_n^2 S_n, \qquad (3.46)$$

to obtain the equation of motion

$$-\partial_z^2 S_n + \omega_s'\partial_z S_n = m_{S_n}^2 S_n, \qquad (3.47)$$

where we have defined

$$\omega_s \equiv \Phi(z) + 3\log z, \qquad (3.48)$$

and $(')$ represents differentiation with respect to z. We can eliminate the first derivative of the field S_n and put the equation of motion in Schrödinger-like form with the substitution

$$S_n = \mathrm{e}^{\omega_s/2}s_n. \qquad (3.49)$$

The final equation of motion is now

$$-s_n'' + \left(\tfrac{1}{4}\omega_s'^2 - \tfrac{1}{2}\omega_s'' + \frac{m_X^2}{z^2}\right)s_n = m_{S_n}^2 s_n. \qquad (3.50)$$

Pseudoscalar Sector

The pseudoscalar eigenstates correspond to the pions, the pseudo-Goldstone bosons of chiral symmetry. This sector is the most difficult to analyze because the pseudoscalar field couples to the longitudinal component of the axial-vector field,

$$A_\mu = A_{\mu\perp} + \partial_\mu\varphi. \qquad (3.51)$$

This results in two coupled differential equations, one that comes from varying the action with respect to the pseudoscalar field π, and one that comes from varying with respect to φ. There are also subtleties in the choice of representation, as illustrated above in (3.20-3.21). The various issues involved in analyzing the pseudoscalar sector are discussed in Section 3.2.3.

Vector Sector

We can derive the mass spectrum of the vector ρ mesons by varying the vector field and using the axial gauge condition $V_z = 0$. Varying the action, we find that

$$\begin{aligned}
\delta\mathcal{S}_V &= -\delta\left(\mathrm{e}^{-\Phi}\sqrt{-g}g^{\mu\rho}g^{\nu\sigma}\left(\partial_\mu V_\nu\partial_\rho V_\sigma - \partial_\mu V_\nu\partial_\sigma V_\rho\right) + \mathrm{e}^{-\Phi}\sqrt{-g}g^{zz}g^{\mu\nu}\partial_z V_\mu\partial_z V_\nu\right) \\
&= -\mathrm{e}^{-\Phi}\sqrt{-g}g^{\mu\rho}g^{\nu\sigma}\left(\partial_\mu V_\nu\delta\partial_\rho V_\sigma - \partial_\mu V_\nu\delta\partial_\sigma V_\rho\right) - \mathrm{e}^{-\Phi}\sqrt{-g}g^{zz}g^{\mu\nu}\partial_z V_\mu\delta\partial_z V_\nu \\
&= \mathrm{e}^{-\Phi}a(z)(\partial^2 V_\mu\delta V^\mu - \partial_\mu\partial^\nu V_\nu\delta V^\mu) + \partial_z\left(\mathrm{e}^{-\Phi}a(z)\partial_z V_\mu\right)\delta V^\mu \\
&= \left(\mathrm{e}^{-\Phi}a(z)\partial_\nu\partial^\nu V_\mu + \partial_z\left(\mathrm{e}^{-\Phi}a(z)\partial_z V_\mu\right)\right)\delta V^\mu, \qquad (3.52)
\end{aligned}$$

We can separate out the $z-$dependence of the field using Kaluza-Klein (KK) decomposition

$$V_\mu^n = \sum_{n=0}^{\infty}\mathcal{V}_\mu^n(x)V_n(z), \qquad (3.53)$$

where $V_n(z)$ are the Kaluza-Klein modes. The equation of motion is now one dimensional

$$-\partial_z^2 V_n + \omega'\partial_z V_n = m_{V_n}^2 V_n, \qquad (3.54)$$

where we have defined

$$\omega \equiv \Phi(z) + \log z. \qquad (3.55)$$

We can eliminate the first derivative of the field, bringing the equation of motion into Schrödinger-like form, using the substitution

$$V_n(z) = e^{\omega/2}v_n(z). \qquad (3.56)$$

The equation of motion is now

$$-v_n'' + \left(\frac{1}{4}\omega'^2 - \frac{1}{2}\omega''\right)v_n = m_{V_n}^2 v_n. \qquad (3.57)$$

This is the general method for finding the equations of motion for the various fields. Using the asymptotic form of the dilaton $\Phi = \lambda z^2$, the mass eigenvalues can be found exactly for this model. The equation of motion is now

$$-v_n'' + \left(\lambda z^2 + \frac{3}{4z^2}\right) v_n = m_n^2 v_n. \tag{3.58}$$

The eigenvalues for this equation are $m_n^2 = \lambda(4n+4)$ for $n = 0, 1, 2, 3, \ldots$ The parameter λ is set by matching this trajectory to experimental data.

We can also determine the value of the 5D coupling constant g_5 used in the action (3.19) by analyzing the vector sector. This is done by matching the vector two-point function $\Pi_V(q^2)$ calculated from this model to the calculation from the operator product expansion of QCD [22]. As shown in [15, 39], we calculate the two-point function near the UV boundary. We begin by re-writing (3.52) in the hard-wall case $\Phi' = 0$,

$$\partial_z \left(\frac{1}{z}\partial_z V\mu(q,z)\right) + \frac{q^2}{z} V_\mu(q,z) = 0, \tag{3.59}$$

where $V_\mu(q,z)$ is the 4D Fourier transform of $V_\mu(x,z)$, and we have used the Fourier-transformed version of the Proca equation,

$$\partial_i \partial^i V_\mu(q,z) = -q^2 V_\mu(q,z) \tag{3.60}$$

Evaluating the vector part of the action (3.19) leaves the boundary action

$$\mathcal{S}_b = -\frac{1}{2g_5^2} \int d^4x \left(\frac{1}{z} V_\mu \partial_z V^\mu\right)_{z=\epsilon}, \tag{3.61}$$

where ϵ is a UV boundary close to $z = 0$. We define V_0^μ to be the Fourier-transformed source of the vector current $J^\mu = \bar{q}\gamma_\mu t^a q$ at the UV boundary,

$$V_0^\mu \equiv \int d^4x \mathrm{e}^{iqx} J^\mu. \tag{3.62}$$

Re-writing the vector field in a separable form

$$V^\mu(q,z) = V(q,z) V_0^\mu(q), \tag{3.63}$$

we see that we should choose the UV boundary condition $V^\mu(q,\epsilon) = 1$. Using this separable form, (3.61) becomes

$$\mathcal{S}_b = -\frac{1}{2g_5^2} \int d^4x V_{0\mu} \left(\frac{\partial_z V(q,z)}{z}\right)_{z=\epsilon} V_0^\mu. \tag{3.64}$$

This expression shows why $V(q,z)$ is often known as the *bulk-to-boundary* propagator. Twice differentiating the boundary action with respect to V_0, we obtain the vector current two-point function,

$$\int d^4x \mathrm{e}^{iqx}\langle J^a_\mu(x)J^b_\nu(0)\rangle = \delta^{ab}(q_\mu q_\nu - q^2 g_{\mu\nu})\Pi_V(q^2), \tag{3.65}$$

where

$$\Pi_V(Q^2) = -\frac{1}{g_5^2 Q^2}\left.\frac{\partial_z V(q,z)}{z}\right|_{z=\epsilon}, \tag{3.66}$$

where $Q^2 = -q^2$. In the limit of large Q^2, we can expand $V(q,z)$ near the UV boundary,

$$V(Q,z) = 1 + \frac{Q^2 z^2}{4}\log Q^2 z^2 + \ldots, \tag{3.67}$$

and to first order, the correlation function becomes

$$\Pi_V(Q^2) = -\frac{1}{2g_5^2}\log Q^2. \tag{3.68}$$

Matching to the large-N_c QCD perturbative result,

$$\Pi_V(k^2) = -\frac{N_c}{24\pi^2}\log k^2, \tag{3.69}$$

where N_c is the number of colors, we find that

$$g_5^2 = \frac{12\pi^2}{N_c}. \tag{3.70}$$

In this work, we take $N_c = 3$, and assume that this value is large enough for the large N_c results to hold.

Axial-Vector Sector

The equation of motion for the axial sector is derived using the same method. Varying the action with respect to A_μ and using the axial gauge $A_z = 0$, we get an equation of similar form to (3.52), but with an additional chiral symmetry-breaking term $\chi^2 A_\mu$,

$$\delta\mathcal{S}_A = \left(\mathrm{e}^{-\Phi}a(z)\partial^2 A_\mu + \partial_z\left(\mathrm{e}^{-\Phi}a(z)\partial_z A_\mu\right) + \mathrm{e}^{-\Phi}g_5^2 a(z)^3 v^2 A_\mu\right)\delta A^\mu. \tag{3.71}$$

After KK decomposition,

$$A^n_\mu = \sum_{n=0}^{\infty}\mathcal{A}^n_\mu(x)A_n(z), \tag{3.72}$$

the equation of motion becomes

$$-\partial_z^2 A_n + \omega' \partial_z A_n + \frac{g_5^2 \chi(z)^2}{z^2} = m_{A_n}^2 A_n, \tag{3.73}$$

with ω defined as in (3.55). To put the equation of motion in Schrödinger form, we make the substitution

$$A_n = \mathrm{e}^{\omega/2} a_n, \tag{3.74}$$

yielding

$$-a_n'' + \left(\frac{1}{4}\omega'^2 - \frac{1}{2}\omega'' + g_5^2 \frac{L^2}{z^2}\chi^2(z) \right) a_n = m_{V_n}^2 a_n. \tag{3.75}$$

The only difference from (3.57) is the presence of the z-dependent mass term involving the chiral condensate. The IR asymptotic behavior of the chiral condensate $\chi(z)$ controls the splitting between the vector and axial-vector mesons at large values of n. Experimentally, we see a constant splitting between the squared masses of the a_1 and ρ mesons, which suggests that chiral symmetry is not restored for the higher excitations. In this model, we can see that the difference between the equations of motion (3.57) and (3.75) is given by

$$\Delta m^2 \equiv \left(m_{A_n}^2 - m_{V_n}^2 \right)_{n\to\infty} = g_5^2 \frac{L^2 \chi^2}{z^2} (z \to \infty). \tag{3.76}$$

To obtain a constant mass splitting, this quantity must become a constant as z approaches infinity. This tells us that $\chi \sim z$ in the IR limit.

The significant drawbacks for this simple soft-wall model are the relatively poor modeling of the ground state and lower resonances and the lack of independent spontaneous and explicit chiral symmetry breaking terms.

3.2 Modified Soft-Wall Model

An improvement on the soft-wall model, suggested in [18], is adding higher-order terms of X to the scalar potential, separating the spontaneous and explicit chiral symmetry breaking. The model established in [25] adds a quartic scalar term to the action:

$$\mathcal{S} = \int d^5x \sqrt{-g} e^{-\Phi(z)} Tr \left[|DX|^2 + m_X^2 |X|^2 - \kappa |X|^4 + \frac{1}{2g_5^2}(F_A^2 + F_V^2) \right], \tag{3.77}$$

where κ is a dimensionless parameter to be fit to the data. To obtain the required linear Regge trajectories for the meson spectra, the dilaton field must be quadratic in z in the IR region,

$$\Phi(z \to \infty) = \lambda z^2, \tag{3.78}$$

where λ sets an energy scale for the model that is related to the slope of the Regge trajectories.

3.2.1 Chiral Symmetry Breaking

The chiral symmetry breaking of the model is examined by deriving the equation of motion for the vacuum expectation value of the scalar field X. Varying (3.77) with respect to X, we find

$$\begin{aligned} \delta\mathcal{S}_X &= -2\mathrm{e}^{-\Phi}\sqrt{-g}\,\mathrm{Tr}\Big(g^{MN}\partial_M X\partial_N\delta X + \{A,X\}\{A,\delta X\} \\ &\quad +[V,X][V,\delta X] + m_X^2 X\delta X - 2\kappa X^\dagger X|X|\delta X\Big). \end{aligned} \tag{3.79}$$

Taking the trace, integrating by parts, and using $|X| = \chi(z)/2 + S(x,z)$, we find the variation of the action with respect to the chiral condensate,

$$\delta\mathcal{S}_\chi = \frac{1}{2}\left(\partial_z\left(\mathrm{e}^{-\Phi}\sqrt{-g}g^{zz}\partial_z\chi\right) + \mathrm{e}^{-\Phi}\sqrt{-g}\,m_X^2\chi + \mathrm{e}^{-\Phi}\sqrt{-g}\frac{\kappa}{2}\chi^3\right)\delta\chi. \tag{3.80}$$

Using the AdS metric, we find that the chiral condensate $\chi(z)$ now has a nonlinear equation of motion

$$\partial_z\left(a^3e^{-\Phi}\partial_z\chi(z)\right) - a^5e^{-\Phi}\left(m_X^2\chi(z) - \frac{\kappa}{2}\chi^3(z)\right) = 0, \tag{3.81}$$

which simplifies to

$$\chi'' - \left(\Phi' + \frac{3}{z}\right)\chi' - m_X^2\chi + \frac{\kappa}{2}\chi^3 = 0, \tag{3.82}$$

where $(')$ denotes a derivative with respect to z.

The higher radially excited states of mesons have parallel Regge trajectories. However, the eigenstates of vector ρ mesons and the axial-vector a_1 mesons do not become degenerate at large n, despite having the same spin. This indicates that chiral symmetry is not restored for the higher excitations. As noted in Section 3.1.2, the mass-splitting

between the highly-excited states of the a_1 and ρ mesons is governed by the IR behavior of the chiral condensate field χ,

$$\Delta m^2 \equiv \left(m_{A_n}^2 - m_{V_n}^2\right)_{n\to\infty} = g_5^2 \frac{L^2\chi^2}{z^2}(z \to \infty). \tag{3.83}$$

Because their trajectories are parallel but not equal, we know that this Δm^2 must be a constant. Examining the right-hand side of (3.83), we see that this requirement implies that $\chi(z) \sim z$ for large z. To match the AdS/CFT dictionary discussed in Chapter 1, the chiral condensate must retain the same UV asymptotic form (3.37). A suitable parameterization that matches the expected UV and IR asymptotic behavior was found and justified in [25]

$$\chi(z) = \alpha z + \beta z \tanh(\gamma z^2), \tag{3.84}$$

with the parameters defined as follows

$$\alpha = \frac{\sqrt{3}m_q}{g_5 L}, \qquad \beta = \sqrt{\frac{4\lambda}{\kappa L^2}} - \alpha, \qquad \gamma = \frac{g_5\sigma}{\sqrt{3}\beta}, \tag{3.85}$$

where m_q is the quark mass, σ is the chiral condensate, λ is set by the experimental Regge trajectories, and g_5 is determined by (3.70) as derived Section 3.1.2. For convenience, we will work in units where the AdS curvature radius L is unity. In the small-z limit, the chiral field becomes

$$\begin{aligned} \chi(z \to 0) &= \alpha z + \beta\gamma z^3 \\ &= \frac{\sqrt{3}}{g_5} m_q + \frac{g_5}{\sqrt{3}}\sigma, \end{aligned} \tag{3.86}$$

where $\sqrt{3}/g_5$ is a normalization factor discussed in [22]. It is clear that, up to normalization, (3.86) matches the UV form required by the AdS/CFT dictionary. In the large-z limit, the chiral field becomes

$$\begin{aligned} \chi(z \to \infty) &= (\alpha + \beta) z \\ &= \sqrt{\frac{4\lambda}{\kappa}} z. \end{aligned} \tag{3.87}$$

The chiral field is linear in the IR, as required, and the dimensionless parameter κ introduced in (3.77) becomes the parameter that controls the axial-vector mass splitting.

The quark mass and chiral condensate can each be taken to zero independently, and the non-restoration of chiral symmetry does not depend on either of these parameters. Thus, the spontaneous and chiral symmetry breaking parameters are independent, as desired. Using (3.84) in (3.81) we can solve for the derivative of the dilaton field

$$\Phi' = \frac{1}{a(z)^3\chi'}\left(\partial_z\left(a(z)^3\chi'\right) - a^5\left(m_X^2\chi - \frac{\kappa}{2}\chi^3\right)\right). \tag{3.88}$$

Using (3.84) in (3.88), the asymptotic behavior of the dilaton is found to be

$$\Phi(z\to 0) = \frac{\kappa}{4}\alpha^2 z^2 + \mathcal{O}(z^6), \tag{3.89}$$

$$\Phi(z\to \infty) = \frac{\kappa}{4}(\alpha+\beta)^2 z^2 = \lambda z^2, \tag{3.90}$$

where the boundary condition $\Phi(0) = 0$ is chosen to ensure a pure AdS metric in the UV limit. We can see that the desired IR dilaton behavior is recovered by this parameterization.

3.2.2 Meson Spectra

Using these parameterizations for the dilaton and chiral condensate fields, we can now calculate the mass eigenvalues of the scalar, vector, and axial-vector mesons. Equations of motion are then derived using the method of Section 3. Due to the more complicated forms for χ and Φ, the eigenvalues are not analytically solvable, so a numerical shooting method is used to calculate the mass spectra for the scalar, vector, and axial-vector sectors. For details on the shooting method, see Appendix A. The mass spectra resulting from this model for the f_0, ρ, and a_1 mesons can be found in [25].

Scalar Mesons

The mass spectrum of the scalar f_0 mesons is determined by deriving the equations of motion for the scalar field $S(x,z)$ and calculating its eigenvalues. The procedure is similar to that delineated in Section 3.1.2, but the quartic term in the scalar potential in (3.77) causes the fluctuations of the scalar field to couple to its own vacuum expectation value. Using a Kaluza-Klein decomposition

$$S(x,z) = \sum_{n=0}^{\infty} \mathcal{S}_n(x)S_n(z), \tag{3.91}$$

we vary the action (3.77) with respect to S, yielding

$$\partial_z(a^3(z)\mathrm{e}^{-\Phi}\partial_z S_n(z)) - a^5(z)\mathrm{e}^{-\Phi}\left(m_X^2 - \frac{3}{2}\kappa\chi^2(z)\right)S_n(z) = -a^3(z)\mathrm{e}^{-\Phi}m_{S_n}^2 S_n(z), \tag{3.92}$$

The scalar equation of motion (3.92) can be brought into a Schrödinger-like form with the substitution

$$S_n(z) = \mathrm{e}^{\omega_s/2}s_n(z), \tag{3.93}$$

with ω_s as defined in (3.48). The eigenvalue equation becomes

$$-\partial_z^2 s_n(z) + \left(\frac{1}{4}\omega_s'^2 - \frac{1}{2}\omega_s'' - \frac{3}{2}\frac{\kappa\chi^2(z)}{z^2} - \frac{3}{z^2}\right)s_n(z) = m_{S_n}^2 s_n(z), \tag{3.94}$$

with the boundary conditions

$$\lim_{z_0\to 0} s_n(z_0) = 0, \qquad \partial_z s_n(z\to\infty) = 0. \tag{3.95}$$

Vector Mesons

The mass spectrum of the vector ρ mesons is found by deriving the equation of motion for the vector field $V(x,z)$ and solving for its eigenvalues. The vector field does not mix with the vacuum expectation value of the scalar field, so the form of equation of motion for the vector mesons is unchanged from (3.57). The only difference in the analysis of this sector is that the functional form for Φ' is much more complicated, so the eigenvalue problem must be solved with the computational shooting method. Because the dilaton field's IR behavior is unchanged, the large-n excitations follow the same linear Regge trajectory as found in Section 3.1.2, but the lower states differ.

Axial-Vector Mesons

The mass spectrum of the axial-vector a_1 mesons is calculated by deriving the equation of motion for the axial-vector field $A(x,z)$ and determining its eigenvalues. The axial-vector field mixes with the chiral condensate field through its kinetic term. This mixing term is unaffected by the change to the scalar potential, so the equation of motion keeps the same form as in (3.75). Again, the behavior of the chiral and dilaton fields is too complicated for analytical solution, so the axial eigenvalues are found with a computational shooting method.

3.2.3 Pions in Modified Soft-Wall Model of AdS/QCD

The mass spectrum for the pseudoscalar mesons was not found in the original paper [25] because the equations of motion are coupled, second order differential equations, and because of some subtleties that arise when considering the representation of the pseudoscalar field. The paper [40] attempted to circumvent these problems by reducing the equations of motion to a single second-order equation, solvable by the shooting method, but their results seemed to miss certain essential features of the pion spectrum. The authors later address this apparent discrepancy in [41]. This modified soft-wall model was later completed in a paper to which the author contributed, [4], which clarified the discrepancies between two common representations of the pseudoscalar field, calculated the pion mass spectrum to good accuracy, and derived the Gell-Mann–Oakes–Renner relation from the model.

As mentioned above, the field X contains both the field representing the scalar mesons, $S(x,z)$, and the field representing the pseudoscalars, $\pi(x,z)$, as well as a non-trivial z-dependent vacuum expectation value, $\chi(z)$. There are two common ways to represent this field:

$$X_e = \left(\frac{\chi(z)}{2} + S(x,z)\right) I e^{2i\pi_e(x,z)^a t^a} \tag{3.96}$$

$$X_l = \left(\frac{\chi(z)}{2} + S(x,z)\right) I + i\pi_l(x,z)^a t^a \tag{3.97}$$

with I the $N_f \times N_f$ identity matrix and t^a the $SU(N_f)$ generators. We will refer to X_e as the exponential representation and X_l as the linear representation. Apparent differences between the representations arise as we note that π_e and π_l are of different dimension. In addition, the linear representation has a quartic interaction term in the Lagrangian, in contrast to the exponential representation. Despite these differences, we will show that the equations of motion derived from each representation are equivalent.

Exponential Representation

Let us take (3.97) and substitute it into (3.77), keeping terms that include the field $\pi(x,z)$, as well as terms that will mix with π,

$$\mathcal{L}_e = -\sqrt{-g}\mathrm{e}^{-\Phi(z)}\frac{1}{2}\delta^{ab}\Big(g^{MN}(\chi^2\,\partial_M\pi\partial_N\pi + \chi^2 A_M A_N - 2\chi^2\partial_M\pi A_N)$$

$$+\frac{g^{MP}g^{NR}}{g_5^2}(\partial_M A_N \partial_P A_R - \partial_M A_N \partial_R A_P)\Big) + \dots \tag{3.98}$$

We work in the axial gauge, $A_z = 0$, and separate the action (3.98) into four-dimensional components and z-dependent terms,

$$\begin{aligned}\mathcal{L}_e &= -\frac{1}{2}\mathrm{e}^{-\Phi(z)}\Big[\sqrt{-g}\, g^{\mu\nu}\left(\chi^2\partial_\mu\pi\partial_\nu\pi + \chi^2 A_\mu A_\nu - 2\chi^2\partial_\mu\pi A_\nu\right)\\ &\quad +\sqrt{-g}g^{zz}\chi^2\partial_z\pi\partial_z\pi \ + \frac{\sqrt{-g}g^{\mu\nu}g^{\rho\sigma}}{g_5^2}(\partial_\mu A_\rho\partial_\nu A_\sigma - \partial_\mu A_\rho\partial_\sigma A_\nu)\\ &\quad +\frac{\sqrt{-g}g^{zz}g^{\mu\nu}}{g_5^2}(\partial_z A_\mu\partial_z A_\nu)\Big].\end{aligned} \tag{3.99}$$

We separate A_μ into its transverse and longitudinal components: $A_\mu = A_{\mu\perp} + \partial_\mu\varphi$, where $\partial_\mu A_\perp^\mu = 0$. Expressing the action in terms of the longitudinal component, φ gives

$$\begin{aligned}\mathcal{L}_e &= -\frac{1}{2}\mathrm{e}^{-\Phi(z)}\Big[\sqrt{-g}g^{\mu\nu}(\chi^2\partial_\mu\pi\partial_\nu\pi + \chi^2\partial_\mu\varphi\partial_\nu\varphi - 2\chi^2\partial_\mu\pi\partial_\nu\varphi)\\ &\quad +\sqrt{-g}g^{zz}\chi^2\partial_z\pi\partial_z\pi \ + \frac{\sqrt{-g}g^{zz}g^{\mu\nu}}{g_5^2}(\partial_z\partial_\mu\varphi\partial_z\partial_\nu\varphi)\Big].\end{aligned} \tag{3.100}$$

Varying (3.100) with respect to π gives

$$\delta\mathcal{L}_e = \partial_z\mathrm{e}^{-\Phi}\sqrt{-g}\, g^{zz}\chi^2\partial_z\pi\delta\pi + \mathrm{e}^{-\Phi}\sqrt{-g}\,\chi^2 g^{\mu\nu}\partial_\nu\partial_\mu(\pi-\varphi)\delta\pi. \tag{3.101}$$

Using a Kaluza-Klein decomposition,

$$\pi(x,z) = \sum_n \Pi_n(x)\pi_n(z), \tag{3.102}$$

$$\varphi(x,z) = \sum_n \Phi_n(x)\varphi_n(z), \tag{3.103}$$

and Proca's equation

$$\partial^2\Pi_n(x) = m_n^2\Pi_n(x)\,, \qquad \partial^2\Phi_n(x) = m_n^2\Phi_n(x)\,, \tag{3.104}$$

we can express the system of equations in terms of its z-dependent parts

$$e^\Phi\partial_z\left(\frac{e^{-\Phi}\chi^2}{z^3}\partial_z\pi_n\right) + \frac{\chi^2 m_n^2}{z^3}(\pi_n - \varphi_n) = 0. \tag{3.105}$$

Varying (3.100) with respect to φ and breaking it down into KK modes gives the second equation of motion

$$\mathrm{e}^\Phi\partial_z\left(\frac{\mathrm{e}^{-\Phi}}{z}\partial_z\varphi_n\right) + \frac{g_5^2L^2\chi^2}{z^3}(\pi_n - \varphi_n) = 0. \tag{3.106}$$

As usual, we express (3.105) and (3.106) in a Schrödinger-like form,

$$\pi \rightarrow \mathrm{e}^{f(z)}\pi \qquad f(z) = \Phi(z) + \log\frac{z^3}{\chi(z)^2} \tag{3.107}$$

$$\varphi \rightarrow \mathrm{e}^{\omega(z)}\varphi \qquad \omega(z) = \Phi(z) + \log z. \tag{3.108}$$

After simplifying, the equations of motion become

$$-\pi_n'' + \left(\frac{\Phi'^2}{4} - \frac{\Phi''}{2} - \frac{\Phi'\chi'}{\chi} + \frac{3\Phi'}{2z} + \frac{15}{4z^2} - \frac{3\chi'}{\chi z} + \frac{\chi''}{\chi} - m_n^2\right)\pi_n = -m_n^2\frac{\chi^2 L^2}{z^2}\varphi_n \tag{3.109}$$

$$-\varphi_n'' + \left(\frac{\Phi'^2}{4} - \frac{\Phi''}{2} + \frac{\Phi'}{2z} + \frac{3}{4z^2} + \frac{g_5^2\chi^2L^2}{z^2}\right)\varphi_n = g_5^2\pi_n \tag{3.110}$$

Linear Representation

When considering the linear representation of the pseudoscalar field (3.97), there are terms quadratic and quartic in π that were not present in the exponential representation. After making the appropriate substitutions in the Lagrangian, it becomes

$$\begin{aligned}\mathcal{L}_l &= -\frac{1}{2}\mathrm{e}^{-\Phi}\sqrt{-g}\Big(g^{\mu\nu}\partial_\mu\pi\partial_\nu\pi + g^{zz}\partial_z\pi\partial_z\pi - 2\chi g^{\mu\nu}\partial_\mu\pi\partial_\nu\varphi + m_X^2\pi^2 - \frac{\kappa}{2}\chi^2\pi^2 \\ &+ g^{\mu\nu}\chi^2\partial_\mu\varphi\partial_\nu\varphi + \frac{g^{\mu\nu}g^{zz}}{g_5^2}\partial_z\partial_\mu\varphi\partial_z\partial_\nu\varphi\Big).\end{aligned} \tag{3.111}$$

Following the same procedure as above, we derive two coupled equations. Varying with respect to φ produces

$$\mathrm{e}^{\Phi}\partial_z\left(\frac{\mathrm{e}^{-\Phi}}{z}\partial_z\varphi_n\right) + \frac{g_5^2L^2\chi}{z^3}\left(\pi_n - \chi\varphi_n\right) = 0. \tag{3.112}$$

Varying with respect to π gives the second equation of the linear representation

$$z^3\mathrm{e}^{\Phi}\partial_z\left(\frac{\mathrm{e}^{-\Phi}}{z^3}\partial_z\pi_n\right) - \left(\frac{m_X^2}{z^2} - \frac{\kappa L^2\chi^2}{2z^2}\right)\pi_n + m_n^2\pi_n = m_n^2\chi\varphi_n. \tag{3.113}$$

We can express (3.112) and (3.113) in a Schrödinger-like form as above with the substitutions

$$\pi_n \rightarrow \mathrm{e}^{\omega_s/2}\pi_n \tag{3.114}$$

$$\varphi_n \rightarrow \mathrm{e}^{\omega/2}\varphi_n, \tag{3.115}$$

where ω_s and ω are defined as in (3.48) and (3.55), respectively. Simplifying the equations , we find

$$-\varphi_n'' + \left(\frac{\Phi'^2}{4} - \frac{\Phi''}{2} + \frac{3}{4z^2} + \frac{\Phi'}{2z} + \frac{g_5^2 L^2 \chi^2}{z^2}\right)\varphi_n = \frac{g_5^2 L \chi}{z}\pi_n \tag{3.116}$$

$$-\pi_n'' + \left(\frac{\Phi'^2}{4} - \frac{\Phi''}{2} + \frac{3}{4z^2} + \frac{3\Phi'}{2z} - \frac{\kappa L^2 \chi^2}{2z^2} - m_n^2\right)\pi_n = -m_n^2 \frac{\chi L}{z}\varphi_n \tag{3.117}$$

Representation Equivalence

The choice of representation for the pseudoscalar field should not affect any physical results obtained from the model. It is therefore desirable to show that the equations of motion derived from the two representations are equivalent.

We begin by expanding X_e to first order in the fields

$$\begin{aligned} X_e &= \left(\frac{\chi}{2} + S\right)(1 + 2i\pi_e + \ldots) \\ &= \frac{\chi}{2} + S + i\pi_e \chi. \end{aligned} \tag{3.118}$$

Comparing (3.118) to (3.97), we infer that

$$\pi_e \chi(z) \to \pi_l \tag{3.119}$$

is the relationship between the two representations. Let us substitute $\pi_e \to \pi_l/\chi(z)$ into the equations of motion of the exponential representation and attempt to obtain the equations of motion of the linear representation. The substitution into (3.106) immediately yields

$$\mathrm{e}^{\Phi}\partial_z\left(\frac{\mathrm{e}^{-\Phi}}{z}\partial_z\varphi\right) + \frac{g_5^2\chi}{z^3}(\pi_l - \chi\varphi) = 0, \tag{3.120}$$

which is equivalent to (3.112) as expected.

Demonstrating the equivalence of the other two equations requires a bit more analysis. First we substitute for π_e in (3.105) and simplify the expression,

$$\frac{z^3 \mathrm{e}^{\Phi}}{\chi}\partial_z\left(\frac{\mathrm{e}^{-\Phi}\chi^2}{z^3}\left(\frac{\pi_l'}{\chi} - \frac{\pi_l \chi}{\chi^2}\right)\right) + m_n^2(\pi_l - \chi\varphi) = 0, \tag{3.121}$$

which becomes

$$\pi_l'' - \left(\Phi' + \frac{3}{z}\right)\pi_l' - \frac{\pi_l}{\chi}\left(\chi'' - \Phi'\chi' - \frac{3}{z}\chi'\right) + m_n^2(\pi_l - \chi\varphi) = 0. \tag{3.122}$$

Recalling the equation of motion for $\chi(z)$ (3.81), which does not depend on the pseuodscalar representation:

$$\chi'' - \left(\Phi' + \frac{3}{z}\right)\chi' + \left(\frac{3}{z^2} + \frac{\kappa L^2 \chi^2}{2z^2}\right) v = 0. \tag{3.123}$$

Using (3.123) in (3.122), we find

$$\pi_l'' - \left(\frac{3}{z} + \Phi'\right)\pi_l' + \left(\frac{3}{z^2} + \frac{\kappa L^2 \chi^2}{2z^2}\right)\pi_l + m_n^2\left(\pi_l - \chi\varphi\right) = 0, \tag{3.124}$$

which is equivalent to the other equation of motion of the linear representation (3.113). The equations of motion are equivalent, confirming that physical results do not depend on the representation.

Pseudoscalar Mass Eigenvalues

The mass eigenvalues for the pions can be calculated in either the exponential or linear representation, using the numerical matrix method detailed in Appendix A. However, it turns out that the boundary conditions

$$\pi(z_0 \to 0) = 0 \qquad \partial_z \pi(z \to \infty) = 0 \tag{3.125}$$

$$\varphi(z_0 \to 0) = 0 \qquad \partial_z \varphi(z \to \infty) = 0 \tag{3.126}$$

are easier to enforce using the linear representation (3.97). This may be due to the relation (**??**) and the fact that the chiral field χ also goes to zero in the UV, making it difficult to enforce the boundary condition on π_e simultaneously. The numerical results for the π_l eigenvalues are shown in Table 3.2.

For large-n excitations the numerical technique develops problems with the boundary conditions. As the number of oscillations in the eigenfunctions increase for higher n modes, the routine finds eigenvalues that are skewed to larger values. To uncover the correct asymptotic behavior for large n, we take the large-z limit of (3.116) and (3.117). As n increases, the eigenfunction is largely determined by the behavior of the effective potential at large z. At large z, the VEV and dilaton behave as

$$\chi(z) = (\alpha + \beta) z \equiv \Gamma \frac{z}{L} \tag{3.127}$$

$$\phi(z) = \lambda z^2. \tag{3.128}$$

n	π Data (MeV)	π_l (MeV)	Large-n π_l
1	140	143	-
2	1300 ± 100	1557	-
3	1816 ± 14	1887	-
4	2070*	2095	-
5	2360*	2298	2245
6	-	-	2403
7	-	-	2551

Table 3.2: The observed masses [1] and calculated masses using the linear representations. The large-n limit solutions are valid from $n \approx 4$. From that point onward, the numerical method used is increasingly inaccurate and fails to find the linear Regge trajectories expected. *=Appears only in the further states of [1].

To take the large-z limit of the linear representation, we introduce a new dimensionless parameter, $\xi = \sqrt{\lambda} z$, and expand in ξ. In the linear representation, we find that (3.116) and (3.117) at large ξ become

$$-\pi_k'' + \xi^2 \pi_k = \left(\frac{\kappa \Gamma^2}{2\lambda} - 2 + \frac{m_k^2}{\lambda} \right) \pi_k - \frac{m_k^2 \Gamma}{\lambda} \varphi_k \tag{3.129}$$

$$-\varphi_k'' + \xi^2 \varphi_k = \frac{g_5^2 \Gamma}{\lambda} (\pi_k - \Gamma \varphi_k) \tag{3.130}$$

where $(')$ here indicates differentiation with respect to ξ. This set of equations has the form of coupled harmonic oscillators, the equations of motion of which are

$$-\varphi_k'' + \xi^2 \varphi_k = (2k+1)\varphi_k \tag{3.131}$$

$$-\pi_k'' + \xi^2 \pi_k = (2k+1)\pi_k \qquad k = 0, 1, \ldots. \tag{3.132}$$

We make the reasonable assumption that $\varphi_k = c_k \pi_k$, which ensures that (3.129), and (3.130) have solutions. Using the form of (3.131) and (3.132) to solve for m_k^2, and making use of the fact that $\Gamma^2 = \frac{4\lambda}{\kappa}$, we find

$$m_k^2 = g_5^2 \Gamma^2 + (2k+1)\lambda. \tag{3.133}$$

Until now we have not made use of the fact that, in the AdS metric, $z \geq 0$. Because of this, the eigenfunctions φ_n and π_n describe *half* harmonic oscillators with half as

many modes; therefore, we must take $k \to 2k$. The mass eigenvalues for large n, where $n = k + 1$, in both representations then become

$$m_n^2 = (4n - 3)\lambda + g_5^2\Gamma^2 \qquad n = 4, 5, \ldots \tag{3.134}$$

which are also listed in Table 3.2 and plotted in Figure 3.1. Combining (3.134) and the numerical technique, we obtain all the pseudoscalar eigenvalues. On inspection, we find that this method should be trusted over the numerical routine for $n \geq 4$.

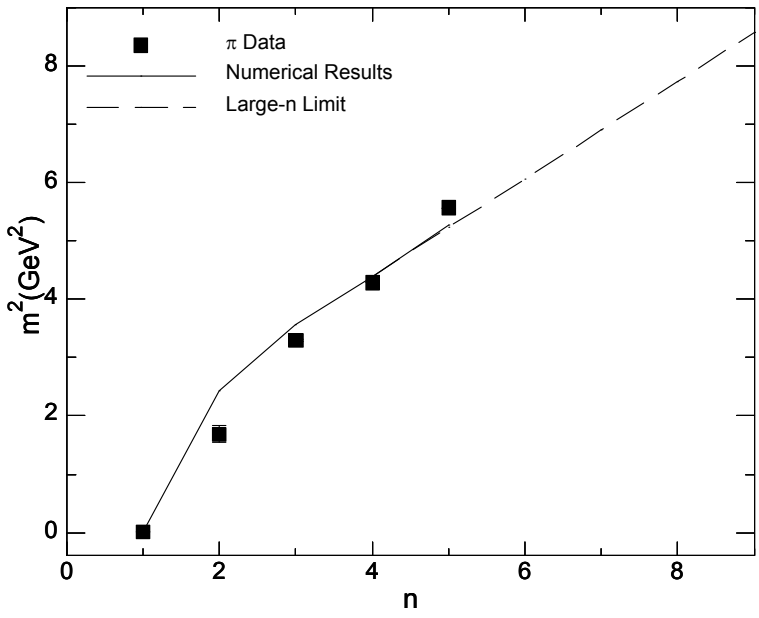

Figure 3.1: The pion mass spectrum calculated in the modified AdS/QCD model is plotted along with the experimental data [1]. The eigenvalues display two important characteristics of the experimental pion spectrum: (1) light ground state and (2) a large gap between the ground state and the first excited state. The large-n mass trajectory clearly follows our calculated eigenvalues from $n \approx 4$ when our numerical routine inadequately follows the oscillations of the higher eigenfunctions.

3.2.4 Gell-Mann–Oakes–Renner Relation

The mass of the ground-state pion is related to the spontaneous breaking of chiral symmetry. Whenever a continuous symmetry is spontaneously broken, a massless particle appears – this result is known as Goldstone's Theorem. The resulting particles are known as Goldstone bosons, or, if the symmetry is also broken explicitly, they are called pseudo-Goldstone bosons because they are not truly massless.

A quark-antiquark pair may spontaneously appear from the vacuum, in keeping with Heisenberg's Uncertainty Principle. This pair will have zero total momentum and angular momentum, resulting that a left-handed quark will be paired with a right-handed antiquark, and vice versa, resulting in a nonzero net chirality. The QCD vacuum contains a condensate of these chiral quark-antiquark states, resulting in a nonzero vacuum expectation value for the chiral operator

$$\langle \bar{q}q \rangle = \langle \bar{q}_L q_R + \bar{q}_R q_L \rangle \neq 0. \tag{3.135}$$

Thus, the vacuum mixes the two quark helicities, causing the light quarks to acquire an effective mass as they move through and interact with the vacuum.

We can explore the relationship of spontaneous chiral symmetry breaking to the pion by parameterizing the matrix element of the axial current $j^{\mu 5}(x)$ between the vacuum and a pion [42]

$$\langle 0|j^{\mu 5}(x)|\pi(p)\rangle = -ip^{\mu} f_{\pi} \mathrm{e}^{-ip\dot{x}}, \tag{3.136}$$

where f_π is known as the *pion decay constant* and has dimensions of mass. In the limit of zero quark mass, the axial current is exactly conserved, i.e. $\partial_\mu j^{\mu 5}(x) = 0$. Taking the derivative ∂_μ of the left-hand side of (3.136) is equivalent to contracting the right-hand side with p_μ, yielding

$$\langle 0|\partial_\mu j^{\mu 5}(x)|\pi(p)\rangle = -p_\mu (ip^{\mu} f_{\pi} \mathrm{e}^{-ip\dot{x}}) = -ip^2 f_{\pi} \mathrm{e}^{-ip\dot{x}} = 0, \tag{3.137}$$

implying that $p^2 = 0$ for the on-shell pion. This can only be true if the pion is massless, as required by Goldstone's theorem.

When the quark masses are not equal to zero, the chiral symmetry is said to be broken explicitly. This is because the QCD Lagrangian contains terms of the form $m_q \bar{q}q = m_q(\bar{q}_L q_R + \bar{q}_R q_L$, which requires a mixing of the chiral components. The axial

field is no longer exactly conserved, becoming

$$\partial_\mu j^{\mu 5}(x) = i\bar{q}\{M, \tau^a\}\gamma^5 q, \tag{3.138}$$

where M is the mass matrix

$$M = \begin{pmatrix} m_u & 0 \\ 0 & m_d \end{pmatrix}. \tag{3.139}$$

Using this equation with 3.137, we find

$$\langle 0|\partial_\mu j^{\mu 5}(0)|\pi(p)\rangle = -p^2 f_\pi \delta^{ab} = \langle 0|i\bar{q}\{M, \tau^a\}\gamma^5 q|\pi^b(p)\rangle. \tag{3.140}$$

NEED TO FINISH GMOR.

We now explore the Gell-Mann–Oakes–Renner relation in the soft-wall AdS/QCD model numerically. Inserting the established equivalence between the exponential and linear representations, $\pi_e = \pi_l/\chi(z)$, into (3.122), we obtain

$$\frac{g_5^2 L^2 \chi^2}{z^2}\partial_z\left(\frac{\pi_l}{\chi}\right) = m_\pi^2 \partial_z \varphi\,. \tag{3.141}$$

Following the method of [15], we construct a perturbative solution in m_π where $\varphi(z) = A(0,z) - 1$ and use the established relation

$$f_\pi^2 = -\,L\frac{\partial_z A(0,z)}{g_5^2 z}\bigg|_{z\to 0.} \tag{3.142}$$

Integrating (3.141) yields

$$\frac{\pi(z)}{\chi(z)} = m_\pi^2 \int_0^z du\, \frac{u^3}{\chi^2(u)}\frac{\partial_z A(0,u)}{g_5^2 u}\,. \tag{3.143}$$

The function $u^3/\chi^2(u)$ has significant support only at small values of $u \sim \sqrt{m_q/\sigma}$, where we may use (3.142) to relate the derivative on $A(0,u)$ to the pion decay constant, so that

$$\frac{\pi_l}{\chi} = -\frac{m_\pi^2 f_\pi^2}{2m_q\sigma}\,. \tag{3.144}$$

We find that letting $\pi_l = -\chi(z)$ solves the axial-vector field's equation of motion

$$\mathrm{e}^{\Phi}\partial_z\left(\frac{\mathrm{e}^{-\Phi}}{z}\partial_z A_\mu(q,z)\right) - \frac{q^2}{z}A_\mu(q,z) - \frac{g_5^2 L^2\chi^2}{z^3}A_\mu(q,z) = 0 \tag{3.145}$$

in the region of small z and as $q \to 0$. As a result, (3.144) becomes the expected Gell-Mann–Oakes–Renner (GOR) relation,

$$2m_q\sigma = m_\pi^2 f_\pi^2 \,. \tag{3.146}$$

We solve for the ground-state pseudoscalar mass, m_π, for differing values of m_q to ensure that the numerical routine respects the GOR relation and gives a reasonable value for f_π. The results are plotted in Figure 3.2. We see linear behavior in the plot, indicating that as $m_q \to 0$ we obtain a constant ratio of m_q/m_π^2. The slope of the line in Figure 3.2 suggests $f_\pi = 90$ MeV, a result consistent with the input parameters as described in [25].

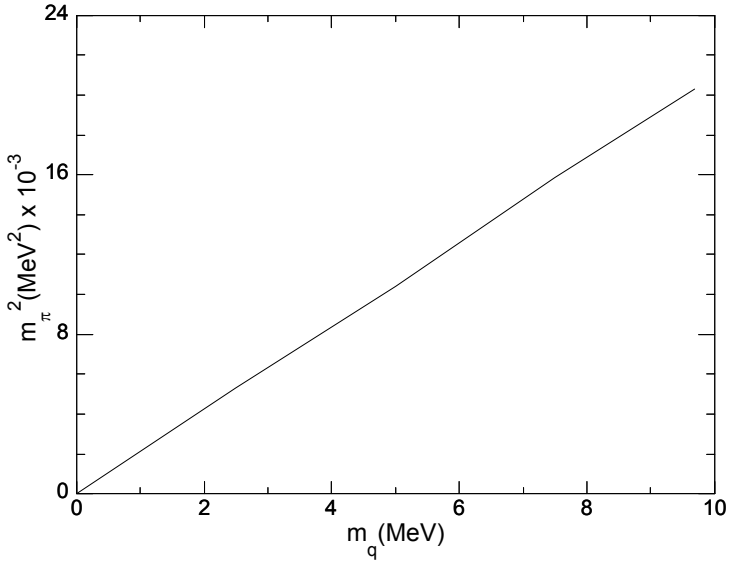

Figure 3.2: Plot of m_π^2 vs m_q yields a straight line from which the pion decay constant f_π is calculated using (3.146).

3.3 Summary

In this chapter, we discussed the metric structure and field content of a soft-wall AdS/QCD model. We illustrated the field content of the simplest such model that

describes light mesons and their spectra. We discussed the vacuum expectation value of the scalar field, which is related to the chiral symmetry breaking of the theory. The behavior of this chiral condensate was derived, and we discussed the shortcomings apparent in the simplest soft-wall models. We then derived the equations of motion for the scalar, vector, and axial-vector mesons.

We also discussed a modified soft-wall model that allows for the correct form of chiral symmetry breaking. In this model, we discussed the derivation of the pseudoscalar equations of motion, and the equivalence between the two common representations of the pseudoscalar field. Finally, we calculated the Gell-Mann–Oakes–Renner relation in the linear representation, showing that it is equivalent to that derived in the exponential representation. We confirmed the Gell-Mann–Oakes–Renner relation numerically in this model, and calculated the value of f_π, in good agreement with the accepted value.

Chapter 4

Dynamical AdS/QCD

"When *I* use a word," Humpty Dumpty said in rather a scornful tone,
"it means just what I choose it to mean – neither more nor less."
Lewis Carroll, *Through the Looking Glass*

In this chapter, we introduce the dynamical approach to soft-wall AdS/QCD, an attempt to be more rigorous than the version of the model discussed in Chapter 3. In the dynamical approach, the background fields including the dilaton and possibly other scalar fields are derived from a gravitational action, rather than parameterized and inserted to the model by hand. We will discuss the basic setup of the model including the necessary and optional terms in the gravitational action. There are a variety of approaches to describing the fields in the dynamical model. We will review the existing literature in this area and motivate the particular dynamical model that is described in detail in Chapter 5.

4.1 Gravity-Dilaton Action

We begin in the so-called string frame, where the geometry is purely AdS_5,

$$ds^2 = \frac{L^2}{z^2}(-dt^2 + dx_i dx^i + dz^2), \tag{4.1}$$

where L is the AdS curvature radius, the index i runs over the three spatial dimensions, and z represents the extra dimension. The minimal gravitational action for a background

dilaton is

$$\mathcal{S} = \frac{1}{16\pi G_5}\int d^5x\sqrt{-g}\mathrm{e}^{-2\Phi}\left(R + \partial_M\Phi\partial^M\Phi - V(\Phi)\right), \tag{4.2}$$

where G_5 is the five-dimensional Newton's constant, R is the Ricci curvature scalar, Φ is the dilaton, and $V(\Phi)$ is some unspecified potential involving the dilaton. The Ricci scalar is defined in Appendix **??**. For the AdS_5 metric, the value of the Ricci scalar is $R = -20/L^2$. The overall constant factor in (4.2) is chosen to satisfy Einstein's equation, as discussed in Appendix **??**.

To derive the equations of motion that result from the gravitational action, it is convenient to perform a conformal transformation to the so-called Einstein frame, where the Ricci scalar appears without being multiplied by the dilaton pre-factor. The transformation to the Einstein frame is

$$g_{MN} = \mathrm{e}^{4\Phi/3}\tilde{g}_{MN}, \tag{4.3}$$

where the tilde distinguishes the Einstein frame.

Let us examine how the conformal transformation affects each term of the action. In the string frame, there is an overall factor of

$$\sqrt{-g} = \sqrt{-\det\left(g^{MN}\right)} = \left(\frac{1}{z}\right)^5 \tag{4.4}$$

In the Einstein frame, the overall factor becomes

$$\sqrt{-g_E} = \left(\frac{\mathrm{e}^{-2\Phi/3}}{z}\right)^5 = \frac{1}{z^5}\mathrm{e}^{-10\Phi/3}. \tag{4.5}$$

Comparing (4.5) to (4.4) it is evident that

$$\sqrt{-g_E} = \mathrm{e}^{-10\Phi/3}\sqrt{-g} \tag{4.6}$$

The potential term has the simplest transformation, where the Einstein potential becomes

$$\tilde{V} = \mathrm{e}^{4\Phi/3}V. \tag{4.7}$$

The Ricci scalar is calculated using the same method as above, resulting in

$$\tilde{R} = -20/L^2 - \frac{4}{\sqrt{6}L^2}z\phi' - \frac{2}{L^2}z^2\phi'^2 - \frac{8}{\sqrt{6}L^2}z^2\phi'' \tag{4.8}$$

The transformation of the dilaton kinetic term is more involved.

The Einstein frame action becomes

$$\mathcal{S}_E = \frac{1}{16\pi G_5}\int d^5x\sqrt{-g_E}\left(\tilde{R} - \tfrac{1}{2}\partial_M\phi\partial_N\phi - \tilde{V}(\phi)\right), \tag{4.9}$$

where the dilaton is re-scaled $\phi = \sqrt{8/3}\Phi$ for a canonical action.

The energy-momentum tensor derived from this action is

$$\begin{aligned} 8\pi G_5 T_{MN} &= \tfrac{1}{2}(\partial_M\phi\partial_N\phi - g_{MN}\mathcal{L}) && (4.10)\\ \mathcal{L} &= \tfrac{1}{2}\partial_\lambda\phi\partial^\lambda\phi + \tilde{V}(\phi) && (4.11)\end{aligned}$$

Two equations of motion are found by varying the Einstein frame action (4.23) with respect to the dilaton and the metric.

$$\begin{aligned} G_{MN} &= 16\pi G_5 T_{MN} && (4.12)\\ \Box\phi &= \frac{\partial\tilde{V}}{\partial\phi}, && (4.13)\end{aligned}$$

where $\Box \equiv \nabla_M\nabla^M$, and ∇_M is the covariant derivative with respect to the metric. It is useful to write (4.12) in the following combinations

$$\begin{aligned} \tilde{g}^{tt}G_{tt} - \tilde{g}^{zz}G_{zz} &= 8\pi G_5(\tilde{g}^{tt}T_{tt} - \tilde{g}^{zz}T_{zz}) = \tfrac{1}{2}\tilde{g}^{zz}\phi'^2, && (4.14)\\ \tilde{g}^{tt}G_{tt} + \tilde{g}^{zz}G_{zz} &= 8\pi G_5(\tilde{g}^{tt}T_{tt} + \tilde{g}^{zz}T_{zz}) = -\tilde{V}(\phi), && (4.15)\end{aligned}$$

where we have made use of the fact that $\tilde{g}^{tt} = -\tilde{g}^{zz}$. Using the energy-momentum tensor defined in (4.10-4.11) and the Einstein metric defined in (4.1) and (4.3), the equations of motion become

$$\begin{aligned} \frac{z^2}{\sqrt{6}}\frac{d}{dz}\left(\frac{1}{z^2}\phi'\right) &= 0. && (4.16)\\ \mathrm{e}^{2\phi/\sqrt{6}}\frac{z^2}{L^2}\left[\frac{\sqrt{6}}{2}\phi'' - \frac{3}{2}\phi'^2 - 3\sqrt{6}\phi' - \frac{12}{z^2}\right] &= \tilde{V}(\phi) && (4.17)\\ \mathrm{e}^{2\phi/\sqrt{6}}\frac{z^2}{L^2}\left[\phi'' - 3\phi'\left(\frac{1}{z} + \frac{\phi'}{\sqrt{6}}\right)\right] &= \frac{\partial\tilde{V}}{\partial\phi}. && (4.18)\end{aligned}$$

Noting that we can re-write (4.7) in terms of the re-scaled dilaton ϕ as $\tilde{V} = \mathrm{e}^{2\phi/\sqrt{6}}V$, we see that (4.17-4.18) can be re-written in terms of the string frame potential

$$\frac{z^2}{L^2}\left[\frac{\sqrt{6}}{2}\phi'' - \frac{3}{2}\phi'^2 - 3\sqrt{6}\phi' - \frac{12}{z^2}\right] = V(\phi) \tag{4.19}$$

$$\frac{z^2}{L^2}\left[\phi'' - 3\phi'\left(\frac{1}{z} + \frac{\phi'}{\sqrt{6}}\right)\right] = \frac{\partial V}{\partial \phi}. \tag{4.20}$$

An obvious limitation of this system is the inability to describe chiral symmetry breaking.

4.2 Gravity-Dilaton-Tachyon Action

A simple extension of the action in (4.2) is simply to include another scalar field in the action. It is hoped that with judicious choices for the behavior of this field, it may be possible to identify it as the chiral condensate field. We add a tachyonic field to the string frame action

$$\mathcal{S} = \frac{1}{16\pi G_5}\int d^5x\sqrt{-g}\mathrm{e}^{-2\Phi}\left(R + \partial_M\Phi\partial^M\Phi - \partial_M\chi\partial^M\chi - V(\Phi,\chi)\right). \tag{4.21}$$

With the same conformal transformation (4.3), we can write the action (4.21) with the Einstein frame metric defined by (4.3). The Ricci scalar, dilaton kinetic term, and potential all transform in the same manner shown in Section 4.1. The transformation of the tachyon field is as follows

$$\begin{aligned}
\sqrt{-g}\mathrm{e}^{-2\Phi}\partial_M\chi\partial^M\chi &= \sqrt{-g}\mathrm{e}^{-2\Phi}g^{MN}\partial_M\chi\partial_N\chi \\
&= \sqrt{-g}\mathrm{e}^{-2\Phi}\left(\mathrm{e}^{-4\Phi/3}\tilde{g}^{MN}\right)\partial_M\chi\partial_N\chi \\
&= \left(\mathrm{e}^{10\Phi/3}\right)\sqrt{-g_E}\mathrm{e}^{-2\Phi}\left(\mathrm{e}^{-4\Phi/3}\tilde{g}^{MN}\right)\partial_M\chi\partial_N\chi \\
&= \sqrt{-g_E}\partial_M\chi\partial^M\chi
\end{aligned} \tag{4.22}$$

The gravity-dilaton-tachyon action in the Einstein frame becomes

$$\mathcal{S}_E = \frac{1}{16\pi G_5}\int d^5x\sqrt{-g_E}\left(\tilde{R} - \tfrac{1}{2}\partial_M\phi\partial^M\phi - \tfrac{1}{2}\partial_M\chi\partial^M\chi - \tilde{V}(\phi,\chi)\right), \tag{4.23}$$

where again $\tilde{V} = \mathrm{e}^{4\Phi/3}V$, and the dilaton is re-scaled $\phi = \sqrt{8/3}\Phi$ for a canonical action.

The energy-momentum tensor derived from this action is similar to that found in (4.10-4.11), with the addition of the tachyon field

$$8\pi G_5 T_{MN} = \tfrac{1}{2}(\partial_M\phi\partial_N\phi + \partial_M\chi\partial_N\chi - g_{MN}\mathcal{L}) \tag{4.24}$$

$$\mathcal{L} = \tfrac{1}{2}\partial_\lambda\phi\partial^\lambda\phi + \tfrac{1}{2}\partial_\lambda\chi\partial^\lambda\chi + \tilde{V}(\phi,\chi). \tag{4.25}$$

Because of the presence of the additional tachyonic field, there is an additional equation of motion in comparison to the model in Section 4.1,

$$\begin{aligned}
\tilde{g}^{tt}G_{tt} - \tilde{g}^{zz}G_{zz} &= 8\pi G_5(\tilde{g}^{tt}T_{tt} - \tilde{g}^{zz}T_{zz}) = \tfrac{1}{2}\tilde{g}^{zz}(\phi'^2 + \chi'^2), && (4.26)\\
\tilde{g}^{tt}G_{tt} + \tilde{g}^{zz}G_{zz} &= 8\pi G_5(\tilde{g}^{tt}T_{tt} + \tilde{g}^{zz}T_{zz}) = -\tilde{V}(\phi) && (4.27)\\
\Box\phi &= \frac{\partial\tilde{V}}{\partial\phi} && (4.28)\\
\Box\chi &= \frac{\partial\tilde{V}}{\partial\chi}. && (4.29)
\end{aligned}$$

Expanding these equations and writing in terms of the string frame potential $V(\phi,\chi)$ yields

$$\begin{aligned}
\frac{z^2}{\sqrt{6}}\frac{d}{dz}\left(\frac{1}{z^2}\phi'\right) &= \chi'^2 && (4.30)\\
\frac{z^2}{L^2}\left[\frac{\sqrt{6}}{2}\phi'' - \frac{3}{2}\phi'^2 - 3\sqrt{6}\phi' - \frac{12}{z^2}\right] &= V(\phi,\chi) && (4.31)\\
\frac{z^2}{L^2}\left[\phi'' - 3\phi'\left(\frac{1}{z} + \frac{\phi'}{\sqrt{6}}\right)\right] &= \frac{\partial V}{\partial\phi} && (4.32)\\
\frac{z^2}{L^2}\left[\chi'' - 3\chi'\left(\frac{1}{z} + \frac{\phi'}{\sqrt{6}}\right)\right] &= \frac{\partial V}{\partial\chi}. && (4.33)
\end{aligned}$$

These equations are not all independent, however. Because the potential does not depend explicitly on the coordinate z, but only through the fields, the total derivative becomes

$$\frac{d}{dz}V(\phi,\chi) = \frac{\partial V}{\partial\phi}\phi'(z) + \frac{\partial V}{\partial\chi}\chi'(z). \tag{4.34}$$

This allows for the elimination of one of (4.32) or (4.33).

Let us examine the behavior of this model when the fields obey a power-law behavior. We make the ansatz

$$\chi(z) = \chi_0 z^n \tag{4.35}$$

for the behavior of the tachyonic field. Inserting this ansatz into (4.30) with the Dirichlet boundary condition $\phi(0) = 0$ gives the solution for ϕ,

$$\phi(z) = \frac{n\sqrt{6}}{12(1+2n)}\chi_0^2 z^{2n}. \tag{4.36}$$

It was shown in [43, 26, 44] that such power-law behavior for the tachyonic field with $n = 3$ or $n = 1$ results in a mass term for χ that implies $m_\chi^2 L^2 = -3$. This is the correct mass for the chiral condensate field that is dual to $\langle \bar{q}q \rangle$. In addition this power-law behavior is exactly the asymptotic behavior that it was argued the chiral field should assume. That is, $\chi \sim z^3$ in the UV limit (in the limit of zero quark mass) and $\chi(z) \sim z$ in the IR limit. This suggests that the tachyonic field can be identified as the chiral condensate.

However, this identification is of limited utility in the gravity-dilaton-tachyon model, as we can see by exploring the IR limit. Letting $n = 1$, we can see that the IR behavior of the dilaton is

$$\phi(z) = \frac{1}{6\sqrt{6}} \chi_0^2 z^2. \tag{4.37}$$

The string frame dilaton is given by $\Phi = \lambda z^2$ in the IR limit, so the re-scaled dilaton becomes $\phi = \sqrt{8/3}\lambda z^2$. We see that the coefficient for the chiral field is determined

$$\chi_0 = 2\sqrt{6}\sqrt{\lambda} \tag{4.38}$$

and the axial-vector mass splitting in this model is set by the equation given in Section **??**

$$\Delta m^2 = \frac{g_5^2 \chi^2}{z^2} (z \to \infty) = g_5^2 \chi_0^2. \tag{4.39}$$

When the phenomenologically determined value for λ is inserted into this equation, the value that is calculated for Δm^2 is too large by an order of magnitude.

Thus, we see that this gravity-dilaton-tachyon system fails because it does not allow separate parameters for the slope of the Regge trajectories and for the axial-vector mass splitting. Further, because (4.30) does not involve the scalar potential, there is no choice for the potential that will rectify this shortcoming of this model.

4.2.1 Alternative Approach to Chiral Symmetry Breaking in Dynamical AdS/QCD

A different approach to including chiral symmetry breaking can be found in [28, 32]. Rather than placing a tachyon in the bulk (closed-string sector), this model keeps the gravity-dilaton action separate from the matter (open-string) sector of the action. In

the string frame, the gravity-dilaton action is written the same as 4.2

$$\mathcal{S}_G = \frac{1}{16\pi G_5}\int d^5x\sqrt{-g}\mathrm{e}^{-2\Phi}\left(R + 4\partial_M\partial^M - V(\Phi)\right), \tag{4.40}$$

while the matter action is written

$$\mathcal{S}_M = -\int d^5x\sqrt{-g}\mathrm{e}^{-\Phi}\mathrm{Tr}\left[|DX|^2 + \frac{1}{2g_5^2}(F_A^2 + F_V^2) + V_M(|X|^2,\Phi)\right], \tag{4.41}$$

where $V_M(|X|^2,\Phi)$ is some potential that could in principle involve both the scalar meson field and the dilaton. The scalar meson field X is a charged field, so it must appear in the potential only with an even exponent. Note the difference in the overall exponential dilaton factor between the two sectors (4.40) and (4.41). This difference is due to the fact that (4.40) governs fields that exist in the bulk, where the strings are closed, and thus have two factors of the string coupling $\lambda^2 \sim \mathrm{e}^{-2\Phi}$. The matter sector is governed by open strings that attach to the N_c D-branes, so have only one factor of the string coupling [**?**].

For the background dynamics, we must take the vacuum expectation value of both sectors and add them

$$\mathcal{S} = \langle\mathcal{S}_G\rangle + \frac{N_f}{N_c}\langle\mathcal{S}_M\rangle. \tag{4.42}$$

The factor of N_f/Nc included above is due to the dynamics of the N_f flavor branes and the N_c color branes. The vacuum expectation value of $\mathcal{S}_G$ is unchanged from (4.40), and

$$\langle\mathcal{S}_M\rangle = -\int d^5x\sqrt{-g}\mathrm{e}^{-\Phi}\left(\tfrac{1}{2}\partial_M\chi\partial^M\chi + V_C(\chi,\Phi)\right), \tag{4.43}$$

where we have defined $V_C = \mathrm{Tr}V_M$.

4.3 Summary

In this chapter, we have introduced dynamical AdS/QCD, an approach intended to put AdS/QCD models on more consistent theoretical footing by deriving the background fields from a potential. We began by developing a simple gravity-dilaton action and showing how to transform between the string and Einstein frames. The equations of motion were derived in the Einstein frame. We also discussed the limitations of a gravity-dilaton model, namely the inability to model chiral symmetry breaking.

We then introduced two models that attempt to include chiral dynamics into a dynamical AdS/QCD model. The first model introduces a tachyon into the bulk, producing a gravity-dilaton-tachyon action. The asymptotic behavior and mass of this tachyonic field are appropriate for that of the chiral condensate field. However, we showed that under this assumption, it is not possible to include a separate parameter for the axial-vector mass splitting, so this model fails to produce the correct axial-vector meson spectrum, irrespective of the choice of scalar potential.

Finally, we introduced a model that introduces the chiral condensate in the open-string sector of the theory. We derived the equations of motion and showed that it is possible to get the correct axial-vector mass splitting if one allows the metric to deviate from anti-de Sitter space in the IR. However, previous work on this model has used a parameterization for the dilaton and chiral condensate fields, and the full scalar potential for this model has not been determined.

In the next chapter, we will introduce a dynamical model of AdS/QCD that includes three background fields in the bulk. This will allow for the correct form of chiral symmetry breaking, and the calculation of all meson spectra. A full expression for the scalar potential will also be derived.

Chapter 5

Dynamical Three-Field Model

Think you're escaping and run into yourself.
Longest way round is the shortest way home.
James Joyce, *Ulysses*

5.1 Review and Motivation

We assume that four-dimensional QCD can be modeled by the following five-dimensional action, written in the string frame:

$$\begin{aligned}\mathcal{S} &= \frac{1}{16\pi G_5}\int d^5x\sqrt{-g}e^{-2\Phi}\Bigg(R+4\partial_M\Phi\partial^M\Phi \\ &\quad -\mathrm{Tr}\left[|DX|^2+\partial_M\mathcal{G}\partial^M\mathcal{G}+\frac{1}{2g_5^2}(F_A^2+F_V^2)+V_m(\Phi,X^2,\mathcal{G})\right]\Bigg)\,. \qquad (5.1)\end{aligned}$$

Here Φ is the dilaton and the metric is pure AdS, $g_{MN}=z^{-2}\eta_{MN}$, with the AdS curvature defined to be unity. The constant $g_5^2=12\pi^2/N_c$, where N_c is the number of colors. The covariant derivative is defined as $D_M=\partial_M+i[V_M,X]-i\{A_M,X\}$. The scalar field X, which is dual to the $\bar{q}q$ operator, obtains a z-dependent vacuum expectation value (VEV)

$$\langle X\rangle=\frac{\chi(z)}{2}I\,, \qquad (5.2)$$

where I is the 2×2 identity matrix. The glueball field $\mathcal{G}$ similarly obtains a z-dependent VEV, $G(z)$. We examine the background dynamics of the fields

$$\mathcal{S} = \frac{1}{16\pi G_5}\int d^5x\sqrt{-g}e^{-2\Phi}\left(R + 4\partial_M\Phi\partial^M\Phi - \tfrac{1}{2}\partial_M\chi\partial^M\chi - \tfrac{1}{2}\partial_M G\partial^M G - V(\Phi,\chi,G)\right), \tag{5.3}$$

where $V = \mathrm{Tr}[V_m]$. The scalar fields Φ, χ, G are dimensionless.

It is easier to search for the background fields in the Einstein frame, where the vacuum action takes the canonical form

$$\mathcal{S}_E = \frac{1}{16\pi G_5}\int d^5x\sqrt{-\tilde{g}}\left(\tilde{R} - \tfrac{1}{2}\partial_M\phi\partial^M\phi - \tfrac{1}{2}\partial_M\chi\partial^M\chi - \tfrac{1}{2}\partial_M G\partial^M G - \tilde{V}(\phi,\chi,G)\right). \tag{5.4}$$

The tilde distinguishes the two frames, with $\tilde{V} = e^{4\Phi/3}V$, and the dilaton is rescaled for a canonical action $\phi = \sqrt{8/3}\Phi$. The string and Einstein frame metrics are related by the conformal transformation

$$g_{MN} = e^{2\phi/\sqrt{6}}\tilde{g}_{MN}\,. \tag{5.5}$$

Previous work showed how to construct a potential for a gravity-dilaton-chiral system without the glueball condensate. We examine the behavior assuming that the fields have power-law behavior, which is accurate in both the UV and IR limits [45]. One of the equations of motion is independent of the choice of potential,

$$\dot{\chi}^2 = \frac{\sqrt{6}}{z^2}\frac{d}{dz}(z^2\dot{\phi})\,. \tag{5.6}$$

To obtain linear confinement, the dilaton should have quadratic behavior in the IR limit, $\phi(z) = \lambda z^2$. The chiral field should have linear behavior in the IR, $\chi(z) = Az$, where A sets the mass splitting between the axial-vector and vector mesons for large radial quantum numbers n. This constant mass-splitting at large n occurs because of the non-restoration of chiral symmetry [46]. Inserting this into (5.6), we find that the chiral field behaves as

$$\chi(z) = 6^{3/4}\sqrt{\lambda}z\,, \tag{5.7}$$

which removes one of the independent parameters of the model in [25]. Using the phenomenological value of λ, which determines the slope of the radial Regge trajectories, we find a mass splitting that is much too large. Because this problem arises in the

equation that is independent of the potential, this issue cannot be resolved by the choice of potential in models that do not consider the glueball condensate. Models that derive the field behavior using the superpotential method suffer from the same problem.

To resolve this problem, we consider the effects of the glueball condensate G on the background equations. This field must be linear in the IR for linear confinement, and behave as $G \sim z^4$ in the UV to match the operator dimension in the AdS/CFT dictionary.

It is noted that the model proposed by Huang and Li [28, 32] accurately represents the non-restoration of chiral symmetry using a model with only two background fields, but their model differs from the work presented here in several respects. They place the meson fields and chiral dynamics in the open-string sector of the model. For linear confinement, this requires that the chiral field approach a constant in the IR, which necessitates a modified metric to obtain the correct chiral dynamics. Our model allows the metric to remain purely AdS in the string frame. Finally, they do not determine an explicit form of the potential, which is the central goal of this work.

5.2 Construction of Potential

Consider the action in the Einstein frame (5.4). To simplify the equations of motion, we use a transformed potential,

$$V = e^{-2\phi/\sqrt{6}}\tilde{V}\,. \tag{5.8}$$

This is simply the potential in the string frame. We re-write it as

$$V = -12 + 4\sqrt{6}\phi + a_0\phi^2 + \frac{m_X^2}{2}\chi^2 + U\,. \tag{5.9}$$

Here U is more than quadratic in the fields. The AdS/CFT dictionary sets the mass for the fields according to the dimension of the dual operator,

$$m^2L^2 = \Delta(\Delta - 4)\,, \tag{5.10}$$

where L is the AdS curvature which we set to unity. The dimension of the $q\bar{q}$ operator is 3, so $m_X^2 = -3/L^2$. The dilaton mass is undetermined and is not connected to

the dimension of the corresponding operator, as discussed in [45]. It is related to the parameter a_0 by $a_0 = \frac{1}{2}\left[(m_\phi L)^2 - 8\right]$. The potential should be an even function of χ.

The equations of motion can be written as

$$\dot{\chi}^2 + \dot{G}^2 = \frac{\sqrt{6}}{z^2}\frac{d}{dz}(z^2\dot{\phi})\,, \tag{5.11}$$

$$U = \tfrac{1}{2}\sqrt{6}z^2\ddot{\phi} - \tfrac{3}{2}(z\dot{\phi})^2 - 3\sqrt{6}z\dot{\phi} - 4\sqrt{6}\phi - a_0\phi^2 + \tfrac{3}{2}\chi^2\,, \tag{5.12}$$

$$\frac{\partial U}{\partial \phi} = 3z\dot{\phi} - 2a_0\phi\,, \tag{5.13}$$

$$\frac{\partial U}{\partial \chi} = z^2\ddot{\chi} - 3z\dot{\chi}\left(1 + \frac{z\dot{\phi}}{\sqrt{6}}\right) + 3\chi\,, \tag{5.14}$$

$$\frac{\partial U}{\partial G} = z^2\ddot{G} - 3z\dot{G}\left(1 + \frac{z\dot{\phi}}{\sqrt{6}}\right)\,. \tag{5.15}$$

We assume that the potential has no explicit dependence on the coordinate z, so the equations 5.13-5.15 are not independent, and we can eliminate one.

5.2.1 Infrared Limit

The requirement of linear confinement requires a solution in the large z limit of the form

$$\phi = \lambda z^2\,, \tag{5.16}$$

$$\chi = Az\,, \tag{5.17}$$

$$G = Bz\,. \tag{5.18}$$

Substitution into (5.11) gives

$$A^2 + B^2 = 6\sqrt{6}\lambda\,. \tag{5.19}$$

The parameter λ is fixed by the slope of the linear trajectory and A is fixed by the axial-vector – vector mass difference. It is useful to write these as

$$A = 6^{3/4}\sqrt{\lambda}\cos\theta\,,$$

$$B = 6^{3/4}\sqrt{\lambda}\sin\theta\,, \tag{5.20}$$

where θ now becomes the parameter controlling the axial-vector – vector mass splitting. Inserting (5.18) into (5.12-5.15) suggests the following terms in our ansatz for the potential

$$U = a_1\phi\chi^2 + a_2\phi G^2 + a_3\chi^4 + a_4 G^4 + a_5\chi^2 G^2 + a_6 G^2\tanh(g\phi)\,. \tag{5.21}$$

We see that there must be a G^2 term in the IR limit, but this is forbidden in the weak-field limit because the glueball condensate field is massless. To circumvent this, we propose the term $G^2\tanh(g\phi)$ with $g > 0$. In the weak field limit this goes to $g\phi G^2$, which is acceptable. The tanh is suggested by 5.8, and it provides a rapid exponential transition from the weak field to the strong field limits that is supported by phenomenology. By substitution one finds the following constraints on the parameters:

$$\begin{aligned} U \to 6 + a_0 + 6\sqrt{6}\left(\cos^2\theta\, a_1 + \sin^2\theta\, a_2\right) \\ +6^3\left(\cos^4\theta\, a_3 + \sin^4\theta\, a_4 + \cos^2\theta\sin^2\theta\, a_5\right) = 0\,, \end{aligned} \tag{5.22}$$

$$\frac{\partial U}{\partial\chi} \to 2a_1 + 24\sqrt{6}\cos^2\theta\, a_3 + 12\sqrt{6}\sin^2\theta\, a_5 + \sqrt{6} = 0\,, \tag{5.23}$$

$$\frac{\partial U}{\partial G} \to 2a_2 + 24\sqrt{6}\sin^2\theta\, a_4 + 12\sqrt{6}\cos^2\theta\, a_5 + \sqrt{6} = 0\,, \tag{5.24}$$

$$\frac{\partial U}{\partial G} \to a_6 = -\tfrac{3}{2}\,. \tag{5.25}$$

We have chosen to exclude (5.13) because it is not independent. The parameter a_6 is determined, and the others will be determined by an examination of the UV limit.

5.2.2 Ultraviolet Limit

Next we look for a solution in the small z limit. The AdS/CFT dictionary dictates that the leading-order UV behavior of the chiral and glueball condensate fields is determined by their dimension. Note also that we are working in the chiral limit where the quark mass is zero. We start by examining only the leading-order terms

$$\chi = \Sigma_0 z^3\,, \tag{5.26}$$

$$G = G_0 z^4\,. \tag{5.27}$$

Substitution into (5.11) and imposing the boundary condition $\phi(0) = 0$ gives

$$\phi = \frac{\sqrt{6}}{28}\Sigma_0^2 z^6 + \frac{\sqrt{6}}{27}G_0^2 z^8 \,. \tag{5.28}$$

Substitution of the desired solution into eqs. (5.12)-(5.15) results in

$$\tilde{U} = -\tfrac{3}{2}(z\dot{\phi})^2 - a_0\phi^2 \tag{5.29}$$

$$\frac{\partial\tilde{U}}{\partial\phi} = \frac{\sqrt{6}}{14}(9-a_0)\Sigma_0^2 z^6 + \frac{2\sqrt{6}}{27}(12-a_0)G_0^2 z^8 \tag{5.30}$$

$$\frac{\partial\tilde{U}}{\partial\chi} = -9\Sigma_0\left(\frac{3}{14}\Sigma_0^2 + \frac{8}{27}G_0^2 z^2\right)z^9 \tag{5.31}$$

$$\frac{\partial\tilde{U}}{\partial G} = -12G_0\left(\frac{3}{14}\Sigma_0^2 + \frac{8}{27}G_0^2 z^2\right)z^{10} \tag{5.32}$$

By substitution one finds the following constraints on the parameters:

$$\frac{\partial\tilde{U}}{\partial\phi} \quad \rightarrow \quad 3a_0 + 7\sqrt{6}a_1 - 27 = 0 \tag{5.33}$$

$$\text{and} \quad 4a_0 + 9\sqrt{6}(a_2 + ga_6) - 48 = 0 \tag{5.34}$$

$$\frac{\partial\tilde{U}}{\partial\chi} \quad \rightarrow \quad \sqrt{6}a_1 + 56a_3 + 27 = 0 \tag{5.35}$$

$$\text{and} \quad \sqrt{6}a_1 + 27a_5 + 36 = 0 \tag{5.36}$$

$$\frac{\partial\tilde{U}}{\partial G} \quad \rightarrow \quad \sqrt{6}(a_2 + ga_6) + 28a_5 + 36 = 0 \tag{5.37}$$

$$\text{and} \quad \sqrt{6}(a_2 + ga_6) + 54a_4 + 48 = 0 \tag{5.38}$$

Using only this leading-order behavior in (5.12-5.15), the system of equations is inconsistent, as there are more equations from matching powers of z than unknown parameters. There are three equations from the IR limit and 6 equations from the UV limit, for a total of nine equations to be solved by only 8 parameters, $a_0 - a_5$, a_8 and g. To solve this problem, consider adding a term $\Sigma_n z^n$ to χ. Substituting into (5.11) and keeping only the lowest-order cross-term we find the additional term in ϕ

$$\Delta\phi = \frac{\sqrt{6}n\Sigma_0\Sigma_n}{(n+4)(n+3)}z^{n+3} \,. \tag{5.39}$$

From (5.12) we find that

$$U = -\tfrac{3}{2}(z\dot{\phi})^2 - a_0\phi^2 + 3\frac{n^3 - 13n + 12}{(n+4)(n+3)}\Sigma_0\Sigma_n z^{n+3}\,. \tag{5.40}$$

Since the ϕ^2 terms start out as z^{12}, z^{14}, z^{16}, and so do the terms in the potential, the n can only take the values 9, 11, etc. This term contributes only to the equation for $\partial U/\partial\chi$.

$$\frac{\partial U}{\partial \chi} = -9\Sigma_0\left(\frac{3}{14}\Sigma_0^2 + \frac{8}{27}G_0^2 z^2\right) z^9 + (n-3)(n-1)\Sigma_n z^n\,. \tag{5.41}$$

By power counting both $n = 9$ and $n = 11$ can contribute.

There could also be higher order terms in G such as $G_m z^m$. This leads to the additional term in ϕ

$$\Delta\phi = \frac{8mG_0G_m}{\sqrt{6}(m+5)(m+4)}z^{m+4}\,. \tag{5.42}$$

It contributes to the equation for $\partial U/\partial G$ as

$$\frac{\partial U}{\partial G} = -12G_0\left(\frac{3}{14}\Sigma_0^2 + \frac{8}{27}G_0^2 z^2\right) z^{10} + m(m-4)G_n z^m\,. \tag{5.43}$$

The choice $m = 8$ is not possible as there is no term of the same order to balance it. Terms with $m = 10$ and $m = 12$ are possible. These new terms cannot affect the equation for $\partial U/\partial\phi$ nor can they contribute to the equation for $\partial U/\partial\chi$. Considering higher order terms in both χ and G leads to

$$U = -\tfrac{3}{2}(z\dot{\phi})^2 - a_0\phi^2 + 3\frac{n^3 - 13n + 12}{(n+4)(n+3)}\Sigma_0\Sigma_n z^{n+3} + \frac{4m(m-4)}{m+4}G_0G_m z^{m+4}\,. \tag{5.44}$$

The appearance of these terms can be understood by writing the following schematic expansions.

$$\chi \sim \Sigma_0 z^3 + \Sigma_0^3 z^9 + G_0^2\Sigma_0 z^{11} + \cdots$$

$$G \sim G_0 z^4 + \Sigma_0^2 G_0 z^{10} + G_0^3 z^{12} + \cdots$$

That is, χ is an odd function of Σ_0 and G is an odd function of G_0. These are the symmetries in the equations of motion. They also follow the spirit of the AdS/CFT correspondence in terms of the dimensionality of the operators and the powers of z.

Including now $m = 10$ and 12, and $n = 9$ and 11, we have the following set of equations in the small z limit, where LHS and RHS refer to the left and right sides of

the respective equations:

$$\begin{aligned} U_{\rm LHS} &= 3\Sigma_0^4 z^{12}\left[4\frac{\Sigma_9}{\Sigma_0^3}-\frac{(54+a_0)}{2^3\cdot 7^2}\right] \\ &+ \frac{1}{7}\Sigma_0^2 G_0^2 z^{14}\left[120\frac{G_{10}}{\Sigma_0^2 G_0}+120\frac{\Sigma_{11}}{\Sigma_0 G_0^2}-\frac{(72+a_0)}{9}\right] \\ &+ 2G_0^4 z^{16}\left[12\frac{G_{12}}{G_0^3}-\frac{(96+a_0)}{3^5}\right], \end{aligned} \tag{5.45}$$

$$\begin{aligned} U_{\rm RHS} &= \Sigma_0^4 z^{12}\left[\frac{\sqrt{6}}{28}a_1+a_3\right] \\ &+ \Sigma_0^2 G_0^2 z^{14}\left[\frac{\sqrt{6}}{27}a_1+\frac{\sqrt{6}}{28}(a_2+ga_6)+a_5\right] \\ &+ G_0^4 z^{16}\left[\frac{\sqrt{6}}{27}(a_2+ga_6)+a_4\right]. \end{aligned} \tag{5.46}$$

$$\left(\frac{\partial U}{\partial \chi}\right)_{\rm LHS} = 3\Sigma_0^3 z^9\left[-\frac{9}{14}+16\frac{\Sigma_9}{\Sigma_0^3}\right]+8\Sigma_0 G_0^2 z^{11}\left[-\frac{1}{3}+10\frac{\Sigma_{11}}{\Sigma_0 G_0^2}\right], \tag{5.47}$$

$$\left(\frac{\partial U}{\partial \chi}\right)_{\rm RHS} = \Sigma_0^3 z^9\left[\frac{\sqrt{6}}{14}a_1+4a_3\right]+\Sigma_0 G_0^2 z^{11}\left[\frac{2\sqrt{6}}{27}a_1+2a_5\right]. \tag{5.48}$$

$$\left(\frac{\partial U}{\partial G}\right)_{\rm LHS} = 6\Sigma_0^2 G_0 z^{10}\left[-\frac{3}{7}+10\frac{G_{10}}{\Sigma_0^2 G_0}\right]+32G_0^3 z^{12}\left[-\frac{1}{9}+3\frac{G_{12}}{G_0^3}\right], \tag{5.49}$$

$$\left(\frac{\partial U}{\partial G}\right)_{\rm RHS} = \Sigma_0^2 G_0 z^{10}\left[\frac{\sqrt{6}}{14}(a_2+ga_6)+2a_5\right] \tag{5.50}$$

$$+ G_0^3 z^{12}\left[\frac{2\sqrt{6}}{27}(a_2+ga_6)+4a_4\right]. \tag{5.51}$$

Altogether, from both the UV and IR limits, there are ten independent equations for the twelve parameters $a_0 - a_6$, Σ_9, Σ_{11}, G_{10}, G_{12}, and g. We take g as the free parameter to use as the rate of transition from small z to large z. The parameters in the potential are found to be

$$a_0 = \frac{3}{2}\frac{1}{6+\sin^2\theta}\left[120+62\sin^2\theta+63\sqrt{6}g\sin^2\theta\right], \tag{5.52}$$

$$a_1 = -\frac{3\sqrt{6}}{4}\frac{1}{6+\sin^2\theta}\left[12+8\sin^2\theta+9\sqrt{6}g\sin^2\theta\right], \tag{5.53}$$

$$a_2 = -\frac{\sqrt{6}}{4}\frac{1}{6+\sin^2\theta}\left[32+24\sin^2\theta+3\sqrt{6}g(9\sin^2\theta-2)\right], \tag{5.54}$$

$$2a_3\cos^2\theta + a_5\sin^2\theta = \frac{1}{24}\frac{1}{6+\sin^2\theta}\left[24 + 22\sin^2\theta + 27\sqrt{6}g\sin^2\theta\right], \tag{5.55}$$

$$2a_4\sin^2\theta + a_5\cos^2\theta = \frac{1}{24}\frac{1}{6+\sin^2\theta}\left[20 + 22\sin^2\theta + 3\sqrt{6}g(9\sin^2\theta - 2)\right], \tag{5.56}$$

$$a_6 = -\frac{3}{2}. \tag{5.57}$$

The coefficients a_0, a_1, a_2 and a_6 are determined, while there are two equations for the three coefficients a_3, a_4 and a_5. That leaves a_5 as a free parameter, to be fit numerically, along with g, θ, G_0, Σ, and λ.

5.3 Numerical Solution

Using the potential discussed, we seek a numerical solution that simultaneously satisfies the UV and IR limits. We use equations (5.11, 5.14, 5.15), which allows for an additional term in the potential, ΔU, such that

$$\frac{\partial}{\partial\chi}\Delta U = \frac{\partial}{\partial G}\Delta U = 0, \tag{5.58}$$

which will be determined from the numerical solution.

The differential equations represent a stiff system, and treatment of the problem as an initial value problem leads to numerical instabilities. We treat it instead as a boundary value problem, using Dirichlet boundary conditions at both boundaries. A relaxation method is used in combination with input approximations for the background fields, which are then iterated to find a stable solution to the system with the given boundary conditions. Because the system is nonlinear, the solution found is not guaranteed to be unique.

The IR boundary is chosen to be sufficiently large to capture the infrared behavior and to give accurate Regge behavior for the large-n radial excitations of the mesons. The UV boundary should approach zero, but it cannot reach zero because of the singularity in the equations of motion. This becomes a problem because equation (5.11) allows constant and divergent terms

$$\Delta\phi(z) = c_1 + c_2 z^{-1}. \tag{5.59}$$

Symbolically, these terms can be set to zero by enforcing the Dirichlet boundary condition $\phi(0) = 0$, but this is impossible to enforce numerically. Creative choice of UV

boundary conditions can eliminate one, but not both, of these unwanted terms without affecting the chiral and glueball fields. The behavior of the numerical solutions suggests that the desired UV behavior is an unstable solution to the equations, and therefore difficult or impossible to find with this iterative method.

As an alternative to direct solution, we parameterize the fields as follows:

$$\Psi(z) = \psi(z)_{UV} f(z) + \psi(z)_{IR} \left(1 - f(z)\right) . \tag{5.60}$$

Here $f(z)$ is some function that transitions smoothly from 1 at small values of z to 0 at large z, while $\psi(z)_{xy}$ represents the known UV and IR limits of the fields ϕ, χ, and G. The switching functions need not be the same for each field. We choose

$$f_\phi(z) = e^{-(\beta_1 z)^{10}} , \tag{5.61}$$

$$f_\chi(z) = e^{-(\beta_2 z)^4} , \tag{5.62}$$

$$f_G(z) = e^{-(\beta_3 z)^5} . \tag{5.63}$$

The powers of the exponential are chosen to be greater than the known power-law behavior of the fields in the UV limit so as to not interfere with this behavior. The β_i will be determined by numerical fitting.

The chiral condensate Σ is set using the Gell-Mann–Oakes–Renner relation:

$$(m_u + m_d)\Sigma = f_\pi^2 m_\pi^2 . \tag{5.64}$$

Using $m_\pi = 139.6$ MeV, $f_\pi = 92$ MeV, and $m_u + m_d = 7.0$ MeV yields a value of $\Sigma = (286\,\mathrm{MeV})^3$.

In all, we have eight parameters to be determined numerically. The first constraint is to obtain the best global visual fit to the vector and axial-vector meson spectra. We do not simply do a chi-squared fitting to the experimental data because the measurement error for the ground state ρ meson is so much smaller than for the others that this would effectively act as the only constraint. Second, we seek to minimize the error in the finite-difference approximations to equations 5.11, 5.14, and 5.15. This is done to an accuracy of one part in 10^4.

Three of the parameters are most phenomenologically relevant: λ, which controls the slope of the meson spectra in the large-n limit; θ, which controls the mass splitting between the a_1 and ρ mesons at large n, and β_2, which controls the location of the

"bend" in the a_1 spectrum. For each set of these parameters, the other parameters are determined by a routine that minimizes the error in the equations of motion. The parameters found are shown in Table 5.1.

$\lambda^{1/2}$	304 MeV	β_1	3.04 GeV
$G_0^{1/4}$	552 MeV	β_2	274 MeV
θ	1.44	β_3	558 MeV
g	3.20	a_5	1.63

Table 5.1: Best fit parameters for the phenomenological model. The parameters λ, θ, and β_2 are chosen for the best visual fit to the ρ and a_1 data, with the rest set by minimizing the error in the equations of motion (5.11), (5.14-5.15).

The background fields that are obtained from this analysis are shown in Figures 5.1-5.3. The asymptotic power-law behavior of the fields is evident in the linear portions of the log-log scale plots shown. The "transition" behavior is most evident in the dilaton because of the large value of β_1, which controls the value of z at which the field transitions from the UV limit to the IR limit.

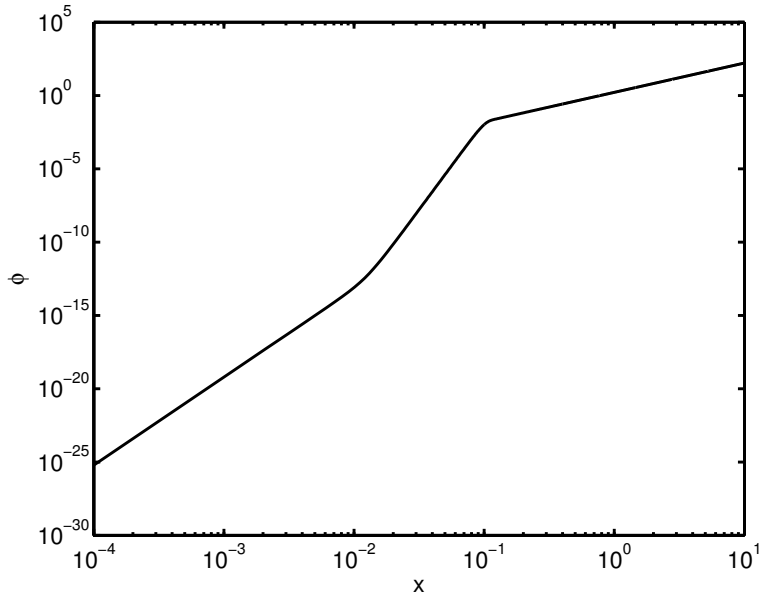

Figure 5.1: A plot of the dilaton field Φ generated by the parameterization (5.62). The UV and IR asymptotic behavior is apparent. The coordinate x is a dimensionless re-scaling of the conformal coordinate, $x = \sqrt{\lambda}z$.

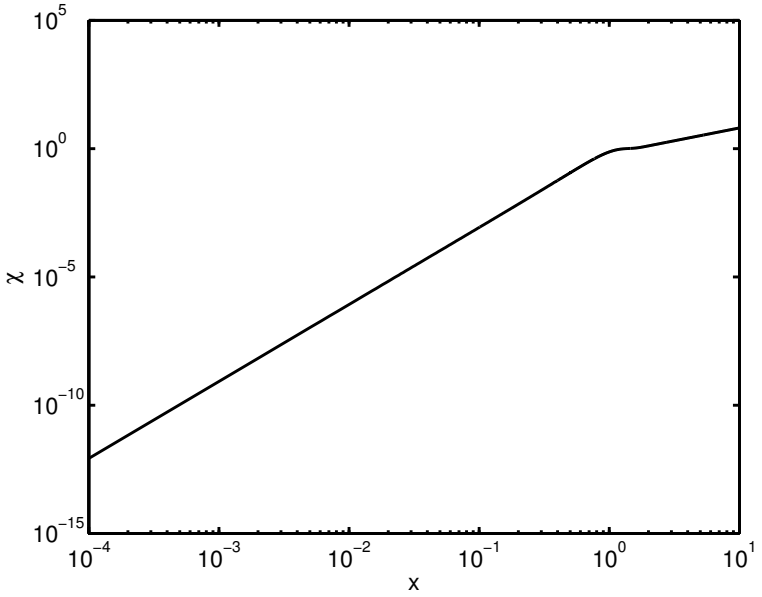

Figure 5.2: A plot of the chiral field χ generated by the parameterization (5.63). The UV and IR asymptotic behavior is apparent, with a rapid transition between them. The coordinate x is a dimensionless re-scaling of the conformal coordinate, $x = \sqrt{\lambda}z$.

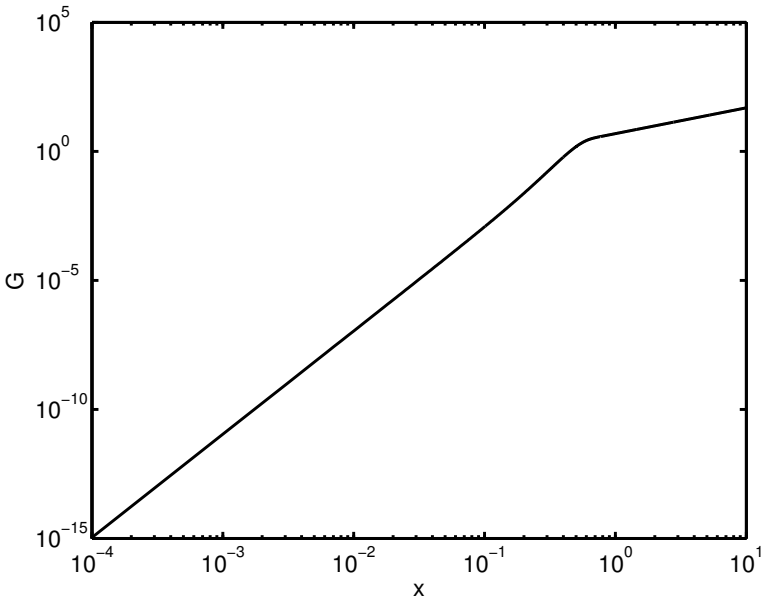

Figure 5.3: A plot of the glueball field G generated by the parameterization (5.63). The UV and IR asymptotic behavior is apparent, with a rapid transition between them. The coordinate x is a dimensionless re-scaling of the conformal coordinate, $x = \sqrt{\lambda} z$.

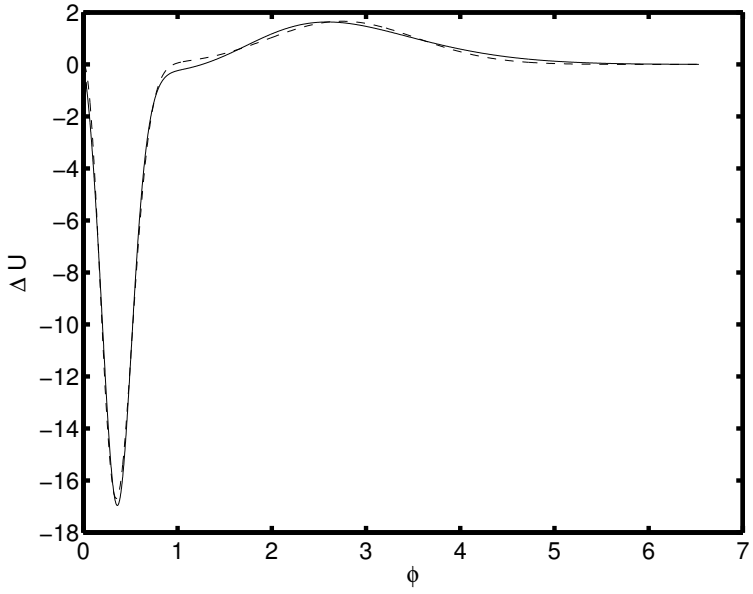

Figure 5.4: Plot of the "extra" term in the potential, $\Delta U(\phi)$. The solid line represents the numerical result, while the dashed line is the fitting of (5.65) using the parameters of Table 5.2.

We now analyze the "extra" term in the potential, ΔU. We obtain this term numerically by subtracting the right-hand side of 5.12 from its left-hand side. This term can be approximated numerically as a function of the dilaton field,

$$\Delta U\left(\phi\right) = \alpha_1 \phi^2 e^{-\left(\phi-\gamma_1\right)^2/\delta_1} + \alpha_2 \phi^2 e^{-\left(\phi-\gamma_2\right)^2/\delta_2}\,. \tag{5.65}$$

The best-fit values for these parameters are shown in Table 5.2. The ΔU as a function of ϕ is shown in Figure 5.4.

α_1	-3.043×10^1	α_2	2.671×10^{-4}
γ_1	7.086×10^{-5}	γ_2	2.213×10^{-2}
δ_1	9.699×10^{-5}	δ_2	1.471×10^{-2}

Table 5.2: The dimensionless parameters for the fitting to ΔU.

5.4 Summary

In this chapter we discussed the construction of a potential for the background fields of a soft-wall AdS/QCD model. The shortcomings of a dynamical AdS/QCD model containing only the dilaton and chiral condensate fields, are alleviated by adding a glueball condensate to the model. We analytically constructed a general potential $U(\phi, \chi, G)$ that recovers the necessary asymptotic behavior of the background fields. Using this as a basis, we numerically constructed a potential that solves the selected background equations to within an accuracy of 10^{-4}. There is an additional allowed term in the potential, $\Delta U(\phi)$, that does not affect the equations that were used in the numerical procedure. This term was found numerically, and fit as a function of the dilaton field.

The potential as constructed here is not guaranteed to be unique. If a different set of the background equations were chosen, the extra term would be expressed as a function of fields other than the dilaton. The parameterization in (5.62-5.63) could also be chosen differently, resulting in a different potential but making little difference to the resulting meson spectra. Finally, terms can be added that do not affect the equations of motion at all, namely, terms which satisfy

$$\Delta U = \Delta\frac{\partial U}{\partial \phi} = \Delta\frac{\partial U}{\partial \chi} = \Delta\frac{\partial U}{\partial G} = 0\,. \tag{5.66}$$

The background fields from this potential can be used to calculate mass spectra for the various light mesons. This work will be presented in the next chapter.

Chapter 6

Meson Spectra

> If it disagrees with experiment it is wrong. In that simple statement is the key to science. It does not make any difference how beautiful your guess is. It does not make any difference how smart you are, who made the guess, or what his name is if it disagrees with experiment it is wrong. That is all there is to it. – Richard Feynman

In this chapter, we calculate the meson spectra for the vector, axial-vector, and pseudoscalar mesons from the dynamical three-field model of AdS/QCD introduced in the preceding chapter. The analysis is much the same as that presented in Chapter 3.

To calculate the spectra of the radial excitations of the mesons, we examine the relevant terms from the string frame action (5.1),

$$\mathcal{S}_{\text{meson}} = -\frac{1}{16\pi G_5}\int d^5x\sqrt{-g}e^{-2\Phi}\text{Tr}\left[|DX|^2 + V_m(\Phi, X^2, \mathcal{G}) + \frac{1}{2g_5^2}\left(F_A^2 + F_V^2\right)\right]. \tag{6.1}$$

The 2×2 field X contains the scalar and pseudoscalar fields (S, π), as well as the VEV. We will use the exponential representation for the scalar field discussed in [4],

$$X_e = \left(S(x,z) + \frac{\chi(z)}{2}\right) I\, e^{2i\pi_e^a(x,z)t^a}, \tag{6.2}$$

where I is the 2×2 identity matrix. The scalar potential V_m does not contribute to the equations of motion for the vector, axial-vector, or pseudoscalar mesons, although terms from the background potential $U(\phi, \chi, G)$ will be useful in the pseudoscalar analysis.

6.1 Vector Sector

We find the equations of motion for the various meson fields by varying the meson action and performing a Kaluza-Klein decomposition. For the vector sector, the equation of motion takes the following form,

$$-\partial_z^2 V_n + \omega' \partial_z V_n = m_{V_n}^2 V_n, \tag{6.3}$$

where we have again defined $\omega \equiv \Phi(z) + \log z$. We can eliminate the first derivative of the field, bringing the equation of motion into Schrödinger-like form, using the substitution

$$V_n(z) = e^{\omega/2} v_n(z). \tag{6.4}$$

The equation of motion is now

$$-v_n'' + \left(\frac{1}{4}\omega'^2 - \frac{1}{2}\omega''\right) v_n = m_{V_n}^2 v_n \tag{6.5}$$

These equations are analytically solvable in the IR limit, giving the same result found in Section 3, but full analysis requires the use of a numerical shooting method to find the mass eigenvalues. This model finds a better phenomenological fit than the results presented in [25], particularly for the ground state ρ meson, as shown in Figure 6.1.

n	ρ experimental (MeV)	ρ model
1	775.5 ± 1	860
2	1282 ± 37	1216
3	1465 ± 25	1489
4	1720 ± 20	1720
5	1909 ± 30	1923
6	2149 ± 17	2107
7	2265 ± 40	2276

Table 6.1: The experimental [1] and predicted values for the masses of the vector mesons.

6.2 Axial-Vector Sector

Varying the action with respect to the axial vector field and performing a KK decomposition,the equation of motion becomes

$$-\partial_z^2 A_n + \omega' \partial_z A_n + \frac{g_5^2 \chi(z)^2}{z^2} = m_{A_n}^2 A_n. \tag{6.6}$$

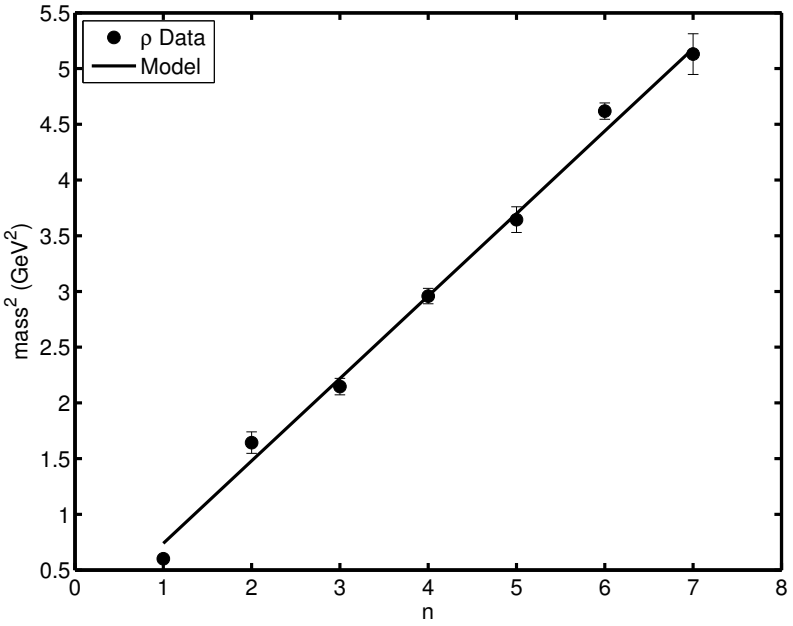

Figure 6.1: Comparison of the predicted mass eigenvalues for the vector sector with the experimental ρ meson spectrum [1].

To put the equation of motion in Schrödinger form, we make the substitution

$$A_n = \mathrm{e}^{\omega/2} a_n, \tag{6.7}$$

yielding

$$-a_n'' + \left(\frac{1}{4}\omega'^2 - \frac{1}{2}\omega'' + g_5^2 \frac{L^2}{z^2}\chi^2(z)\right) a_n = m_{V_n}^2 a_n. \tag{6.8}$$

The results are plotted in Figure 6.2. The model fits the experimental data well, with the large-n states following the linear trajectory, and the "bend" in the a_1 spectrum at $n = 2$, which is controlled by the β_2 parameter that was fit to this data in Section 5.3.

6.3 Pseudoscalar Sector

When using the exponential representation for the scalar field, the terms from the potential do not contribute to the equations of motion for the pion field. This can be

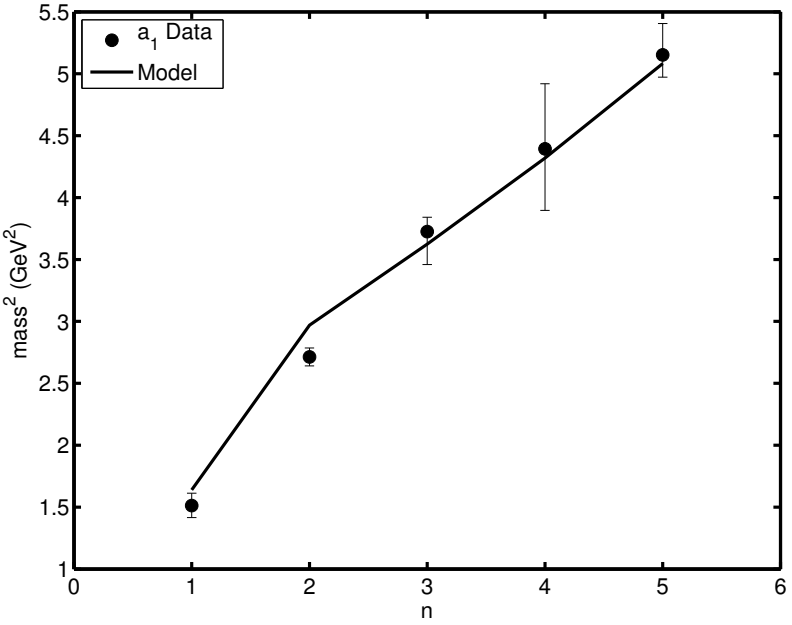

Figure 6.2: Comparison of the predicted mass eigenvalues for the axial-vector sector with the experimental a_1 meson spectrum [1].

easily seen by noting that $|X_e|^n$ does not contain any terms involving the pion field π_e field when n is even. We have required the potential to be an even function of X, so there are no such terms. This would seem to suggest that we use the exponential representation to calculate the pion mass spectrum. However, as noted in [4], π_e is extremely sensitive to boundary conditions, and the numerical results are not reliable. For this reason, we seek to work with an equation of motion written in the linear representation.

For convenience, we begin by deriving the equations of motion in the exponential representation. Working in the axial gauge $A_z = 0$, we rewrite the axial meson field in terms of its perpendicular and longitudinal components: $A_\mu = A_{\mu\perp} + \partial_\mu\varphi$. Only the longitudinal component of the axial field, φ, contributes to the pion equations of motion. We use (6.1), keeping only the relevant terms

$$\mathcal{L} = e^{-2\Phi}\sqrt{-g}\left[\chi^2(\partial_\mu\pi_e\partial^\mu\pi_e + \partial_\mu\varphi\partial^\mu\varphi - 2\partial_\mu\pi\partial^\mu\varphi + \partial_z\pi_e\partial^z\pi_e) + \frac{1}{g_5^2}\partial_z\partial_\mu\varphi\partial^z\partial^\mu\varphi\right]. \tag{6.9}$$

n	a_1 experimental (MeV)	a_1 model
1	1230 ± 40	1280
2	1647 ± 22	1723
3	$1930\ ^{+30}_{-70}$	1904
4	2096 ± 122	2078
5	$2270\ ^{+55}_{-40}$	2254

Table 6.2: The experimental [1] and predicted values for the masses of the axial-vector mesons.

Varying with respect to φ yields

$$e^{2\Phi}\partial_z\left(\frac{e^{-2\Phi}}{z}\partial_z\varphi\right)+\frac{g_5^2\chi^2}{z^3}(\pi_e-\varphi)=0\,, \tag{6.10}$$

while varying π_e gives

$$\frac{e^{2\Phi}z^3}{\chi^2}\partial_z\left(\frac{e^{-2\Phi}\chi^2}{z^3}\partial_z\pi_e\right)+m_n^2(\pi_e-\varphi)=0\,. \tag{6.11}$$

It was shown in [4] that the equations of motion are equivalent under the substitution $\pi_e \to \pi_l/\chi(z)$, so we make the appropriate substitution and expand the equations:

$$-\varphi''+\left(2\Phi'+\frac{1}{z}\right)\varphi'=\frac{g_5^2\chi}{z^2}(\chi\varphi-\pi_l)\,, \tag{6.12}$$

$$-\pi_l''+\left(2\Phi'+\frac{3}{z}\right)\pi_l'+\left(\chi''-2\chi'\Phi'-\frac{3\chi'}{z}\right)\frac{\pi_l}{\chi}=m_n^2(\pi_l-\chi\varphi)\,. \tag{6.13}$$

We can put these equations into Schödinger-like form with the following substitutions:

$$\varphi = e^{\omega/2}\varphi_n\,, \tag{6.14}$$

$$\pi_l = e^{\omega_s/2}\pi_n\,, \tag{6.15}$$

with $\omega = 2\Phi + \ln z$ and $\omega_s = 2\Phi + 3\ln(z)$. This yields

$$-\varphi_n''+\left(\tfrac{1}{4}\omega'^2-\tfrac{1}{2}\omega"+\frac{g_5^2\chi^2}{z^2}\right)\varphi_n=\frac{g_5^2\chi}{z}\pi_n\,, \tag{6.16}$$

$$-\pi_n''+\left(\tfrac{1}{4}\omega_s'^2-\tfrac{1}{2}\omega_s"+\frac{\chi''}{\chi}-\frac{2\chi'\Phi'}{\chi}-\frac{3\chi'}{z\chi}-m_n^2\right)\pi_n=-m_n^2\frac{\chi}{z}\varphi_n\,. \tag{6.17}$$

The dependence of these equations of motion on the scalar potential can be made explicit by using the background equation for the chiral field, written here in the string frame

$$z^2\chi'' - 3z\chi'\left(1+\frac{z\Phi'}{\sqrt{6}}\right) = m_X^2\chi + \frac{\partial U}{\partial\chi}\,. \tag{6.18}$$

Substituting, we can re-write (6.17) as

$$-\pi_n'' + \left(\tfrac{1}{4}\omega_s'^2 - \tfrac{1}{2}\omega_s" + \frac{m_X^2}{z^2} + \frac{1}{z^2}\frac{\partial U}{\partial\chi} - m_n^2\right)\pi_n = -m_n^2\frac{\chi}{z}\varphi_n\,. \tag{6.19}$$

The results are shown in Figure 6.3 and in Table 6.3. It should be emphasized that all parameters were previously determined, so these are truly predictions of the model. The states with mass 2070 and 2360 MeV are listed in the PDG as further states, with less certainty assigned to them. We assume that these should be identified as the $n = 4$ and $n = 6$ states, leaving a vacancy at $n = 5$ for a state still to be observed in future experiments. On the other hand, the PDG has two further states listed as X(2210) with unknown quantum numbers, either of which could be the $n = 5$ state. We include this state in the figure and in the table, but it should be recognized that nothing in our work depends on this very speculative identification.

n	π experimental (MeV)	π model
1	140	0
2	1300 ± 100	1580
3	1816 ± 14	1868
4	2070 ± 35*	2078
5	$2210\ ^{+79}_{-21}$ †	2230
6	2360 ± 25*	2389
7	–	2544
8	–	2686

Table 6.3: The experimental [1] and predicted values for the masses of the pseudoscalar mesons. The states marked with an * appear only in the further states of the PDG. The state marked with a † is an unconfirmed resonance X(2210) with unknown quantum numbers. Whether it really represents the $n = 5$ state is pure speculation.

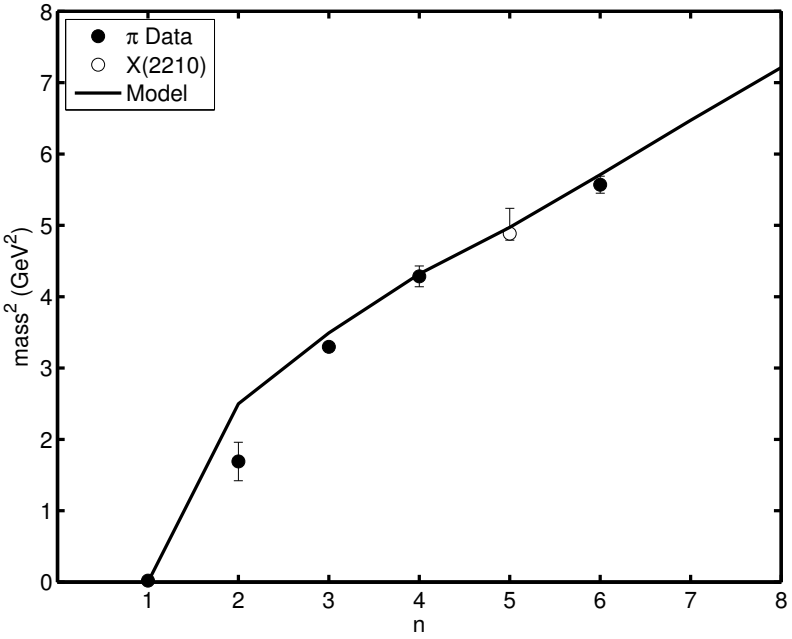

Figure 6.3: Comparison of the predicted mass eigenvalues for the pseudoscalar sector with the experimental π meson spectrum [1]. The states plotted here with $n = 4$ and $n = 6$ are identified as radial excitations of the pion only in the further states of the PDG. The unconfirmed state X(2210), with unknown quantum numbers, is plotted here as the $n = 5$ state of the pion.

6.4 Summary

In this chapter, we calculated the meson spectra for the vector, axial-vector, and pseudoscalar mesons from the dynamical three-field AdS/QCD model discussed in Chapter 5. Portions of the vector and axial-vector spectra were used as inputs for the parameters used in the determination of the potential. While acknowledging theses inputs, the overall goodness of fit is notable.

The pseudoscalar spectrum was not used to set any of the parameters in the model, so it can be regarded as a true prediction. The overall fit to the pion spectrum is quite good. The ground state pion is massless because the quark mass in this model is zero. We have speculatively identified the unconfirmed X(2210) state with unknown quantum numbers as the $n = 5$ pion state. With this identification, and identifying the

pion states from the "further states" section of the PDG as the $n = 4$ and $n = 6$ states, the fit to the higher pion states is excellent. However, nothing in the analysis depends on this extremely tenuous identification.

The f_0 meson spectrum is found by analyzing the fluctuations of the scalar field. However, the scalar field mixes with the glueball field, leading to a more complicated analysis. This analysis will be completed in the following chapter.

Chapter 7

Scalar and Glueball Sectors

The terms of the action relevant for the scalar meson and glueball fields have the form

$$\mathcal{S} = -\frac{1}{16\pi G_5}\int d^5x\sqrt{-g}e^{-2\Phi}\mathrm{Tr}\left[|DX|^2 + \partial_M\mathcal{G}\partial^M\mathcal{G} + V_m(\Phi, X^2, \mathcal{G})\right]. \tag{7.1}$$

Here, we are using the exponential representation for the scalar field,

$$X = \left(S(x,z) + \frac{\chi(z)}{2}\right)e^{2i\pi(x,z)}, \tag{7.2}$$

where $S(x,z)$ is the scalar field fluctuations and $\chi(z)$ is the chiral condensate. The glueball field $\mathcal{G}$ also has a condensate, written as

$$\mathcal{G} = \left(H(x,z) + \frac{G(z)}{2}\right), \tag{7.3}$$

where $H(x,z)$ are the fluctuations of the glueball field and $G(z)$ is the glueball condensate.

The potential V_m is defined in such a way that $\langle \mathrm{Tr}V_m\rangle = V$, where V is the potential for the background fields in the string frame,

$$V = -12 + 4\sqrt{6}\phi + a_0\phi^2 + \frac{m_X^2}{2}\chi^2 + U + \Delta U, \tag{7.4}$$

where ϕ is the re-scaled version of the dilaton, $\phi = \sqrt{8/3}\Phi$. Here, U is more than quadratic in the fields,

$$U = a_1\phi\chi^2 + a_2\phi G^2 + a_3\chi^4 + a_4G^4 + a_5\chi^2G^2 + a_6G^2\tanh(\phi), \tag{7.5}$$

and ΔU is assumed to be a function of ϕ only.

The terms of $\mathrm{Tr}V_m$ that are relevant for the analysis of the scalar sector are those terms involving $X, \mathcal{G}$,

$$\mathrm{Tr}V_m \sim m_X^2 X^2 + 2a_1\phi X^2 + 2a_2\phi\mathcal{G}^2 + 8a_3X^4 + 8a_4\mathcal{G}^4 + 8a_5X^2\mathcal{G}^2 + 2a_6\mathcal{G}^2\tanh g\phi. \quad (7.6)$$

Expanding and keeping only terms that are quadratic in the fields S, H, we obtain

$$\mathrm{Tr}V_m \sim \left(m_X^2 + 2a_1\phi + 12a_3\chi^2 + 2a_5G^2\right)S^2 + \left(2a_2\phi + 12a_4G^2 + 2a_5\chi^2 + 2\tanh(g\phi)\right)H^2 + 4a_5G\chi HS. \quad (7.7)$$

We can simplify the expression by writing

$$\mathrm{Tr}V_m \sim \left(m_X^2 + \frac{\partial^2 U}{\partial\chi^2}\right)S^2 + \frac{\partial^2 U}{\partial G^2}H^2 + 4a_5G\chi HS, \quad (7.8)$$

where

$$\frac{\partial^2 U}{\partial\chi^2} = 2a_1\phi\chi + 4a_3\chi^3 + 2a_5\chi G^2 \quad (7.9)$$

$$\frac{\partial^2 U}{\partial G^2} = 2a_2\phi G + 4a_4G^3 + 2a_5\chi^2 G + 2a_6G\tanh(g\phi) \quad (7.10)$$

The equations of motion are as follows. Varying with respect to S gives the equation of motion

$$\partial_z(z^{-3}e^{-2\Phi}S') - z^{-5}e^{-2\Phi}\left(m_X^2 + \frac{\partial^2 U}{\partial\chi^2}\right)S - 4a_5z^5e^{-2\Phi}G\chi H = -z^3e^{-3}m_S^2S. \quad (7.11)$$

Varying with respect to H yields the equation of motion

$$\partial_z(z^{-3}e^{-2\Phi}H') - z^{-5}e^{-2\Phi}\frac{\partial^2 U}{\partial G^2}H - 4a_5z^5e^{-2\Phi}G\chi S = -z^3e^{-3}m_S^2H. \quad (7.12)$$

To put the equations in Schrödinger form, we make the substitutions

$$S \rightarrow e^{\omega_s/2}S \quad (7.13)$$

$$H \rightarrow e^{\omega_s/2}H, \quad (7.14)$$

where $\omega_s = 2\Phi + 3\log z$. This reduces the equations of motion to

$$-S'' + \left(\tfrac{1}{4}\omega_s'^2 - \tfrac{1}{2}\omega_s'' + m_X^2 - \frac{\partial^2 U}{\partial\chi^2}\right)S + 4a_5G\chi H = m_S^2S \quad (7.15)$$

$$-H'' + \left(\tfrac{1}{4}\omega_s'^2 - \tfrac{1}{2}\omega_s'' - \frac{\partial^2 U}{\partial G^2}\right)H + 4a_5G\chi S = m_H^2H \quad (7.16)$$

These equations need to be solved simultaneously for the eigenvalues m_S^2, m_H^2.

Chapter 8

Conclusion and Discussion

I'll go higher still!
I'll build my throne higher! I can and I will!
I'll call some more turtles. I'll stack 'em to heaven!
I need 'bout five thousand, six hundred and seven!
Dr. Seuss, "Yertle the Turtle"

References

[1] J. Beringer, J. F. Arguin, R. M. Barnett, K. Copic, O. Dahl, D. E. Groom, C. J. Lin, J. Lys, H. Murayama, C. G. Wohl, W. M. Yao, P. A. Zyla, C. Amsler, M. Antonelli, D. M. Asner, H. Baer, H. R. Band, T. Basaglia, C. W. Bauer, J. J. Beatty, V. I. Belousov, E. Bergren, G. Bernardi, W. Bertl, S. Bethke, H. Bichsel, O. Biebel, E. Blucher, S. Blusk, G. Brooijmans, O. Buchmueller, R. N. Cahn, M. Carena, A. Ceccucci, D. Chakraborty, M. C. Chen, R. S. Chivukula, G. Cowan, G. D'Ambrosio, T. Damour, D. de Florian, A. de Gouvêa, T. DeGrand, P. de Jong, G. Dissertori, B. Dobrescu, M. Doser, M. Drees, D. A. Edwards, S. Eidelman, J. Erler, V. V. Ezhela, W. Fetscher, B. D. Fields, B. Foster, T. K. Gaisser, L. Garren, H. J. Gerber, G. Gerbier, T. Gherghetta, S. Golwala, M. Goodman, C. Grab, A. V. Gritsan, J. F. Grivaz, M. Grünewald, A. Gurtu, T. Gutsche, H. E. Haber, K. Hagiwara, C. Hagmann, C. Hanhart, S. Hashimoto, K. G. Hayes, M. Heffner, B. Heltsley, J. J. Hernández-Rey, K. Hikasa, A. Höcker, J. Holder, A. Holtkamp, J. Huston, J. D. Jackson, K. F. Johnson, T. Junk, D. Karlen, D. Kirkby, S. R. Klein, E. Klempt, R. V. Kowalewski, F. Krauss, M. Kreps, B. Krusche, Yu. V. Kuyanov, Y. Kwon, O. Lahav, J. Laiho, P. Langacker, A. Liddle, Z. Ligeti, T. M. Liss, L. Littenberg, K. S. Lugovsky, S. B. Lugovsky, T. Mannel, A. V. Manohar, W. J. Marciano, A. D. Martin, A. Masoni, J. Matthews, D. Milstead, R. Miquel, K. Mönig, F. Moortgat, K. Nakamura, M. Narain, P. Nason, S. Navas, M. Neubert, P. Nevski, Y. Nir, K. A. Olive, L. Pape, J. Parsons, C. Patrignani, J. A. Peacock, S. T. Petcov, A. Piepke, A. Pomarol, G. Punzi, A. Quadt, S. Raby, G. Raffelt, B. N. Ratcliff, P. Richardson, S. Roesler, S. Rolli, A. Romaniouk, L. J. Rosenberg, J. L. Rosner, C. T. Sachrajda, Y. Sakai, G. P. Salam, S. Sarkar, F. Sauli, O. Schneider, K. Scholberg, D. Scott, W. G. Seligman, M. H. Shaevitz, S. R. Sharpe, M. Silari, T. Sjöstrand, P. Skands,

J. G. Smith, G. F. Smoot, S. Spanier, H. Spieler, A. Stahl, T. Stanev, S. L. Stone, T. Sumiyoshi, M. J. Syphers, F. Takahashi, M. Tanabashi, J. Terning, M. Titov, N. P. Tkachenko, N. A. Törnqvist, D. Tovey, G. Valencia, K. van Bibber, G. Venanzoni, M. G. Vincter, P. Vogel, A. Vogt, W. Walkowiak, C. W. Walter, D. R. Ward, T. Watari, G. Weiglein, E. J. Weinberg, L. R. Wiencke, L. Wolfenstein, J. Womersley, C. L. Woody, R. L. Workman, A. Yamamoto, G. P. Zeller, O. V. Zenin, J. Zhang, R. Y. Zhu, G. Harper, V. S. Lugovsky, and P. Schaffner. Review of Particle Physics. *Physical Review D*, 86(1):010001, July 2012.

[2] Yoshifumi Hyakutake. Quantum Near Horizon Geometry of Black 0-Brane. page 34, November 2013, 1311.7526.

[3] Masanori Hanada, Yoshifumi Hyakutake, Goro Ishiki, and Jun Nishimura. Holographic description of quantum black hole on a computer. page 14, November 2013, 1311.5607.

[4] Thomas M. Kelley, Sean P. Bartz, and Joseph I. Kapusta. Pseudoscalar mass spectrum in a soft-wall model of AdS/QCD. *Physical Review D*, 83(1):016002, January 2011, 1009.3009.

[5] Sean P. Bartz and Joseph I. Kapusta. A Dynamical Three-Field AdS/QCD Model. page 17, June 2014, 1406.3859.

[6] Alfonso V. Ramallo. Introduction to the AdS/CFT correspondence. page 64, October 2013, 1310.4319.

[7] a Zaffaroni. Introduction to the AdS-CFT correspondence. *Classical and Quantum Gravity*, 17(17):3571–3597, September 2000.

[8] Youngman Kim, Ik Jae Shin, and Takuya Tsukioka. Holographic QCD: Past, Present, and Future. *Progress in Particle and Nuclear Physics*, page 80, May 2012, 1205.4852.

[9] J. Erdmenger, N. Evans, I. Kirsch, and E. J. Threlfall. Mesons in gauge/gravity duals. *The European Physical Journal A*, 35(1):81–133, February 2008, 0711.4467.

[10] Edward Witten. Bound states of strings and p-branes. *Nuclear Physics B*, 460(2):335–350, February 1996, 9510135.

[11] Gary T. Horowitz and Andrew Strominger. Black strings and p-branes. *Nuclear Physics B*, 360(1):197–209, August 1991.

[12] Andreas Karch and Emanuel Katz. Adding flavor to AdS/CFT. *Journal of High Energy Physics*, 2002(06):043–043, June 2002, 0205236.

[13] T. Sakai and S. Sugimoto. Low Energy Hadron Physics in Holographic QCD. *Progress of Theoretical Physics*, 113(4):843–882, April 2005, 0412141.

[14] T. Sakai and S. Sugimoto. More on a Holographic Dual of QCD. *Progress of Theoretical Physics*, 114(5):1083–1118, November 2005, 0507073.

[15] Joshua Erlich, Emanuel Katz, Dam Son, and Mikhail Stephanov. QCD and a Holographic Model of Hadrons. *Physical Review Letters*, 95(26):261602, December 2005, 0501128.

[16] Leandro Da Rold and Alex Pomarol. Chiral symmetry breaking from five-dimensional spaces. *Nuclear Physics B*, 721(1-3):79–97, August 2005, 0501218.

[17] Leandro Da Rold and Alex Pomarol. The scalar and pseudoscalar sector in a five-dimensional approach to chiral symmetry breaking. *Journal of High Energy Physics*, 2006(01):157–157, January 2006, 0510268.

[18] Andreas Karch, Emanuel Katz, Dam Son, and Mikhail Stephanov. Linear confinement and AdS/QCD. *Physical Review D*, 74(1):015005, July 2006, 0602229.

[19] Nick Evans and Andrew Tedder. Perfecting the ultra-violet of holographic descriptions of QCD. *Physics Letters B*, 642(5-6):546–550, November 2006, 0609112.

[20] H. Grigoryan and A. Radyushkin. Structure of vector mesons in a holographic model with linear confinement. *Physical Review D*, 76(9):095007, November 2007, 0706.1543.

[21] Herry Kwee and Richard Lebed. Pion form factor in improved holographic QCD backgrounds. *Physical Review D*, 77(11):115007, June 2008, 0712.1811.

[22] Aleksey Cherman, Thomas Cohen, and Elizabeth Werbos. Chiral condensate in holographic models of QCD. *Physical Review C*, 79(4):045203, April 2009, 0804.1096.

[23] P. Colangelo, F. De Fazio, F. Giannuzzi, F. Jugeau, and S. Nicotri. Light scalar mesons in the soft-wall model of AdS/QCD. *Physical Review D*, 78(5):17, July 2008, 0807.1054.

[24] Song He, Mei Huang, Qi-Shu Yan, and Yi Yang. Confront Holographic QCD with Regge Trajectories of vectors and axial-vectors. page 9, October 2007, 0710.0988.

[25] Tony Gherghetta, Joseph Kapusta, and Thomas Kelley. Chiral symmetry breaking in the soft-wall AdS/QCD model. *Physical Review D*, 79(7):076003, April 2009, 0902.1998.

[26] Brian Batell and Tony Gherghetta. Dynamical soft-wall AdS/QCD. *Physical Review D*, 78(2):026002, July 2008, 0801.4383.

[27] Danning Li and Mei Huang. Dynamical holographic QCD model: resembling renormalization group from ultraviolet to infrared. November 2013, 1311.0593.

[28] Danning Li and Mei Huang. Dynamical holographic QCD model for glueball and light meson spectra. *Journal of High Energy Physics*, 2013(11):88, November 2013, 1303.6929.

[29] Wayne de Paula, Tobias Frederico, Hilmar Forkel, and Michael Beyer. Dynamical holographic QCD with area-law confinement and linear Regge trajectories. *Physical Review D*, 79(7):075019, April 2009, 0806.3830.

[30] W. de Paula and T. Frederico. Scalar mesons within a dynamical holographic QCD model. *Physics Letters B*, 693(3):287–291, October 2010, 0908.4282.

[31] Qi Wang and An Min Wang. Chiral Symmetry Breaking in the Dynamical Soft-Wall Model. page 4, January 2012, 1201.3349.

[32] Danning Li, Mei Huang, and Qi-Shu Yan. A dynamical soft-wall holographic QCD model for chiral symmetry breaking and linear confinement. *The European Physical Journal C*, 73(10):2615, October 2013, 1206.2824.

[33] Andreas Karch, Emanuel Katz, Dam T Son, and Mikhail A Stephanov. On the sign of the dilaton in the soft wall models. *Journal of High Energy Physics*, 2011(4):66, April 2011, 1012.4813.

[34] Juan M. Maldacena. The Large N Limit of Superconformal Field Theories and Supergravity. *Advances in Theoretical Mathematical Physics*, 2:20, November 1997, 9711200.

[35] Igor R. Klebanov and Edward Witten. Ads/CFT correspondence and symmetry breaking. *Nuclear Physics B*, 556(1-2):89–114, September 1999, 9905104.

[36] S.S. Gubser, I.R. Klebanov, and A.M. Polyakov. Gauge theory correlators from non-critical string theory. *Physics Letters B*, 428(1-2):105–114, May 1998, 9802109.

[37] Edward Witten. Anti De Sitter Space And Holography. *Adv.Theor.Math.Phys.*, 2:253–291, February 1998, 9802150.

[38] Peter Breitenlohner and Daniel Z. Freedman. Positive energy in anti-de Sitter backgrounds and gauged extended supergravity. *Physics Letters B*, 115(3):197–201, September 1982.

[39] Hyun-Chul Kim and Youngman Kim. Quark-gluon mixed condensate of the QCD vacuum in holographic QCD. *Journal of High Energy Physics*, 2008(10):011–011, October 2008, 0808.3639.

[40] Yan-Qin Sui, Yue-Liang Wu, Zhi-Feng Xie, and Yi-Bo Yang. Prediction for the mass spectra of resonance mesons in the soft-wall AdS/QCD model with a modified 5D metric. *Physical Review D*, 81(1):014024, January 2010, 0909.3887.

[41] Yan-Qin Sui, Yue-Liang Wu, and Yi-Bo Yang. Predictive AdS/QCD Model for Mass Spectra of Mesons with Three Flavors. *Physical Review D*, 83(6):065030, March 2011, 1012.3518.

[42] D. Peskin, M. and Schroeder. An Introduction to Quantum Field Theory. 1995.

[43] Todd Springer. *Hydrodynamics of strongly coupled non-conformal fluids from gauge/gravity duality.* Ph.d. thesis, University of Minnesota, August 2009, 0908.1587.

[44] S. S. Afonin. Holographic like models as a five-dimensional rewriting of large-Nc QCD. *International Journal of Modern Physics A*, 25(31):33, January 2010, 1001.3105.

[45] J. I. Kapusta and T. Springer. Potentials for soft-wall AdS/QCD. *Physical Review D*, 81(8):086009, April 2010, 1001.4799.

[46] M. Shifman and A. Vainshtein. Highly excited mesons, linear Regge trajectories, and the pattern of the chiral symmetry realization. *Physical Review D*, 77(3):034002, February 2008, 0710.0863.

Appendix A

Numerical Methods for solving Ordinary Differential Equations

Ordinary differential equations can always be reduced to a system of coupled first-order differential equations, which is advantageous for numerical solutions. For example, the second-order equation

$$y''(x) + f(x)y'(z) = g(x) \tag{A.1}$$

can be rewritten as

$$y'(x) = z(x) \tag{A.2}$$

$$z'(x) = g(z) - f(x)z(x) \tag{A.3}$$

Written generically, an ordinary differential equations system is reduced to a set of N first-order differential equations

$$y_i'(x) = f_i(x, y1, \ldots, y_N) \qquad i = 1, \ldots, N \tag{A.4}$$

where the functions f_i are some known set of equations involving the coordinate x and the dependent variables y_i. For a unique solution, one must specify a set of N boundary conditions. If these conditions are all specified at a single point, x_0, this is known as an initial value problem, and one can simply choose an integration method and calculate the values for f_i over the desired domain. When some of the conditions are specified at point x_0 and the rest are specified at the point x_f, this is known as a boundary value problem, and one must use one of the methods detailed below.

A.1 Shooting Method

The shooting method turns boundary value problems into initial value problems. The classic example of a shooting method can be visualized as the firing of a cannon, with boundary conditions given by the location of the cannon and the location of the target. This is changed to an initial value problem by selecting an arbitrary value for the angle of the cannon and firing. The angle of the cannon is incremented until the cannonball hits the target, which matches the final boundary condition.

More concretely, the boundary value problem is written as in (A.4), with boundary conditions

$$B_{1j}(x_0, y_1, \ldots, y_N) = 0 \qquad j = 1, \ldots, n_1 \tag{A.5}$$

$$B_{2k}(x_f, y_1, \ldots, y_N) = 0 \qquad k = 1, \ldots, n_2 \tag{A.6}$$

with n_1 boundary conditions at point x_0 and $n_2 = N - n_1$ at point x_f. These boundary conditions generically can be any algebraic combination of the variables.

For concreteness, consider a second-order eigenvalue problem of the type considered in this thesis,

$$\psi_n''(z) + V(z)\psi_n(z) = m_n^2 \psi_n(z). \tag{A.7}$$

This can be reduced to two first-order differential equations by making the substitutions $y_1 = \psi$, $y_2 = \psi'$, resulting in the system

$$y_1' = y_2 \tag{A.8}$$

$$y_2' = \left(m_n^2 - V(z)\right) y_1. \tag{A.9}$$

The boundary conditions are $y_1(z_0) = y_1(z_f) = 0$. [1] In this instance, the eigenvalues are of greater importance than the behavior of the solutions y_1, y_2, so the overall normalization of the solutions is arbitrary.

This boundary value problem is changed to an initial value problem by setting

$$y_1(z_0) = 0 \tag{A.10}$$

$$y_2(z_0) = c, \tag{A.11}$$

[1] In the soft-wall model, we should take the limit $z_f \to \infty$. This is impossible to do numerically, but it is easy to make z_f sufficiently large that the eigenvalues are not effected.

where c is an arbitrary constant. A small test value for m_n is chosen, and the initial value problem is solved.

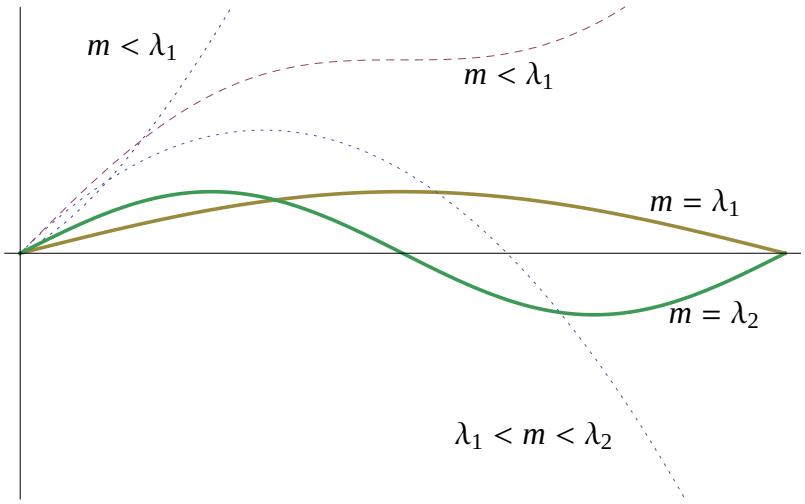

Figure A.1: An illustration of the shooting method.

As illustrated in Figure A.1, when the test value for m_n is less than the first eigenvalue λ_1, the value of $y_1(x_f)$ is positive. As m_n is incremented, eventually $y_1(x_f)$ becomes negative. A root-finding routine is used to approximate the values λ_n such that $y_1(x_f) = 0$. The number of antinodes in the wavefunction indicates to which excitation mode the eigenvalue corresponds.

A.2 Matrix Method

The coupled second-order The equations of motion can be reduced to a set of second-order differential equations,

$$-\varphi'' + V_1(z)\varphi + f(z)\pi = 0, \tag{A.12}$$

$$-\pi'' + V_2(z)\pi + g(z)\varphi = 0, \tag{A.13}$$

where the eigenvalues are contained within the coefficient functions. These equations can be expressed as a system of first-order differential equations

$$\Phi' + W(z)\Phi = 0, \tag{A.14}$$

where W is the matrix

$$W = \begin{pmatrix} 0 & 1 & 0 & 0 \\ V_1(z) & 0 & f(z) & 0 \\ 0 & 0 & 0 & 1 \\ g(z) & 0 & V_2(z) & 0 \end{pmatrix} \tag{A.15}$$

and Φ is the vector

$$\Phi_{\alpha i} = \begin{pmatrix} \varphi_i \\ -\varphi_i' \\ \pi_i \\ -\pi_i' \end{pmatrix} \tag{A.16}$$

that forms an orthonormal basis of solutions. We can propagate the solution Φ between two boundary points

$$\Phi(z_f) = U(z, z_f, z_0, m_n^2)\Phi(z_0), \tag{A.17}$$

where we solve (A.14) with the appropriate boundary condition at z_0. The eigenvectors and eigenvalues of U are then calculated. Two of the solutions are divergent, but the solutions that correspond to the two smaller eigenvalues do not diverge. We label the non-divergent solutions as the eigenvectors u_3 and u_4. The non-divergent solutions for Φ_i can be written as a linear combination of u_3 and u_4

$$\Phi_i = \alpha u_3 + \beta u_4. \tag{A.18}$$

Non-trivial values of α and β satisfy

$$\begin{pmatrix} u_3^1 & u_4^1 \\ u_3^3 & u_4^3 \end{pmatrix} \begin{pmatrix} \alpha \\ \beta \end{pmatrix} = 0 \tag{A.19}$$

for Dirichlet or

$$\begin{pmatrix} u_3^2 & u_4^2 \\ u_3^4 & u_4^4 \end{pmatrix} \begin{pmatrix} \alpha \\ \beta \end{pmatrix} = 0 \tag{A.20}$$

for Neumann boundary conditions. The values of m_n^2 that minimize the determinant of the matrix (A.19) or (A.20) are the eigenvalues of the system (A.12-A.13). An abrupt change in its behavior of the plot of the determinant vs. the value of m_n signals the location of an eigenvalue.